

Quantum information of optical magnetometry: Semiclassical Cramer-Rao bound violation and Heisenberg scaling

Georg Engelhardt,^{1,*} Ming Li,² Xingchang Wang,³ JunYan Luo,⁴ and J.F. Chen^{3,1}

¹*Shenzhen International Quantum Academy, Shenzhen 518048, China*

²*Shenzhen Institute for Quantum Science and Engineering,*

Southern University of Science and Technology, Shenzhen 518055, China

³*Department of Physics, Southern University of Science and Technology, Shenzhen 518055, China*

⁴*Department of Physics, Zhejiang University of Science and Technology, Hangzhou 310023, China*

(Dated: January 6, 2026)

Optical magnetometers use the rotation of linearly polarized laser light induced by the Faraday effect for high precision magnetic field measurements. Here, we carry out an in-depth quantum information investigation, deploying two distinct models: The first, semiclassical model can violate the quantum Cramer-Rao bound by several orders of magnitude for weak dissipation and large atom numbers, invalidating the semiclassical approach in this parameter regime. The second model, describing the atoms as a collective spin, respects the Cramer-Rao bound for all parameters. Interestingly, the collective model also predicts Heisenberg scaling for the quantum Fisher information. The comparison of both models shows that Heisenberg scaling is a result of measurement-induced quantum correlation in an otherwise non-interacting quantum system. As the Heisenberg scaling appears in a stationary state of a macroscopic quantum system, it can be thus viewed as a new paradigm in quantum sensing. Intriguingly, the comparison of both models with experimental data can constitute a test for the foundations of quantum mechanics in a macroscopic ensemble of atoms.

I. INTRODUCTION

Spectroscopy offers highly precise methods in quantum sensing [1, 2], such as for optical clocks [3–5], electric-field sensing with Rydberg atoms [6–10], and entanglement-enhanced spectroscopy [11–14]. Optical magnetometers, which look back on a decades-long history, are highly precise spectroscopic quantum sensing devices featuring many scientific and technological applications [15–19]. They offer a highly controllable platform for sensing magnetic fields [20–25], and testing fundamental quantum properties of the light-matter interaction [26–28]. These magnetometers are currently deployed in the search for dark matter in the galactic halo [29–31], and to improve gravitational wave detectors [32–35]. The basic magnetometer setup is sketched in Fig. 1(a), where the polarization direction of linearly-polarized light is rotated when propagating through an atomic vapor. The rotation is thereby determined by the magnetic-field-dependent state of the atoms, whose level structure is sketched in Fig. 1(b).

According to quantum information theory, the celebrated quantum Cramer-Rao inequality [36–38],

$$\langle \Delta \hat{X}^2 \rangle \geq \frac{1}{\mathcal{I}_X^{(Q)}}, \quad (1)$$

sets a fundamental bound for the precision $\langle \Delta \hat{X}^2 \rangle$ of the parameter to measured (X) in terms of the quantum Fisher information $\mathcal{I}_X^{(Q)}$ [39]. The Heisenberg limit

refers to the quadratic scaling of the quantum Fisher information as a function of time or system size, surpassing thus the standard quantum limit, referring to linear scaling, observed in typical measurement protocols [40]. The desired Heisenberg scaling has been predicted for several many-body quantum systems utilizing quantum criticality [41–45], a squeezed or entangled initial state [46–49], precisely coordinated quantum operations [50, 51], and quantum error correction [52–54]. There is also increasing research attention on continuous quantum sensing [55–59]. While the sensitivity of optical magnetometry has been frequently investigated [60–64], often involving phenomenological assumptions, a thorough quantum information analysis in terms of the Fisher information is currently missing.

As this article demonstrates, the quantum information analysis of optical magnetometers operating with a hot atomic vapor reveal nontrivial insights into these established quantum sensing devices, suggesting that the operation in the Heisenberg limit is feasible. Even more, it can test the foundations of quantum mechanics in macroscopic quantum system consisting of 10^{10} entities by probing the validity of the Cramer-Rao bound. The objective of this work is twofold: (i) Develop the required theoretical concepts and methods necessary for a meaningful quantum information analysis of spectroscopic quantum sensing devices; (ii) Apply this methodology to analyze the quantum information of an established protocol in optical magnetometry. These two objectives are approached as follows:

(i) To ensure that the light-matter interaction is described on a solid footing, we invoke a quantum trajectory approach [65–67], which is capable of microscopically describing continuous quantum measurements [68–70]. To get direct access to spectroscopic observables,

* georg-engelhardt-research@outlook.com

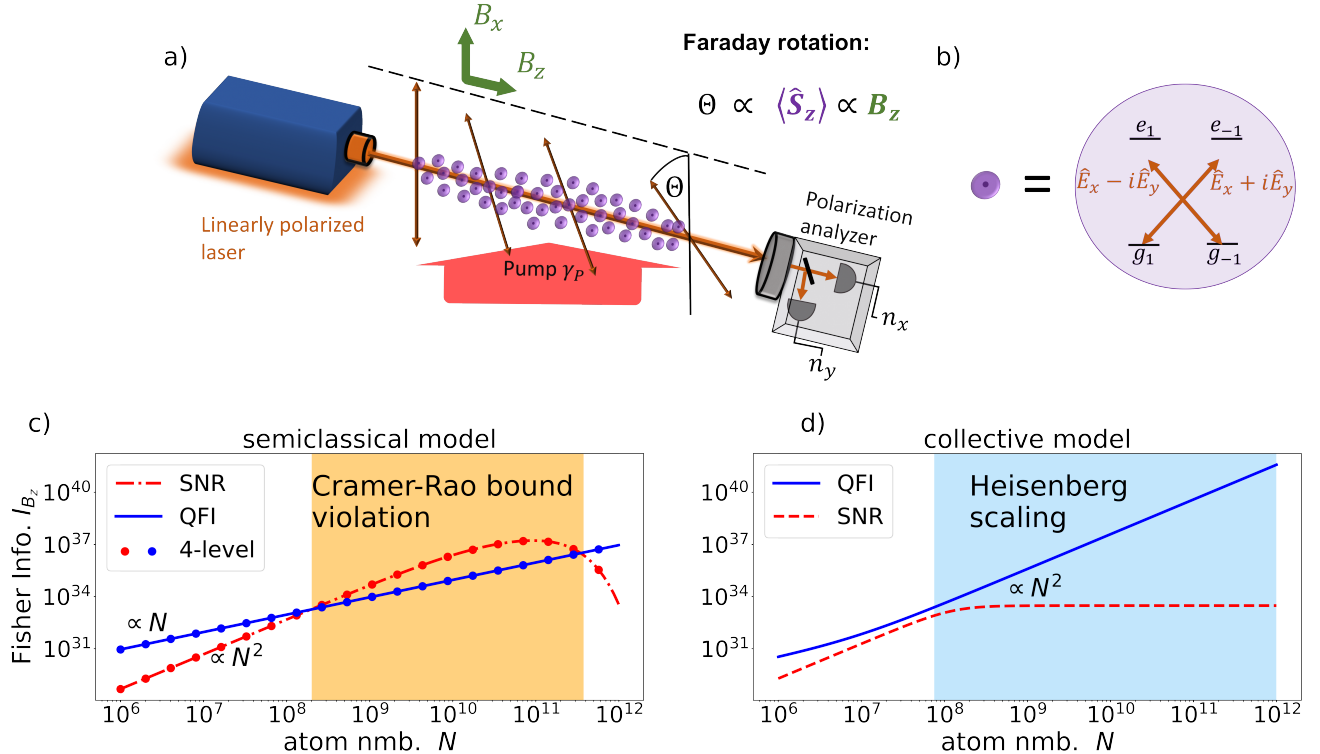


FIG. 1. (a) Sketch of the optical magnetometer, which utilizes the rotation of linearly polarized laser light induced by the light-matter interaction with an atomic vapor to estimate the strength of the magnetic field B_z . (b) Four-level scheme of the atoms in the vapor in the z basis, including the atomic transitions induced by the linearly-polarized laser. (c) Fisher information calculated for the ground-state manifold in the semiclassical model (colored lines). For large atom numbers, the signal-to-noise ratio (SNR) of the measured probability distribution can exceed the quantum Fisher Information (QFI), giving rise to a semiclassical Cramer-Rao bound (CRB) violation. The predictions are confirmed by the calculations in the semiclassical four-level system (dashed black). (d) Fisher information for the collective model, in which the Cramer-Rao bound is maintained. Overall parameters are explained in Sec. III, and $B_z = 0$.

we amend the quantum trajectories with full-counting statistics [67], allowing to describe the system on the ensemble level instead of simulating stochastic quantum trajectories. Facing a macroscopic ensemble of atoms, we investigate this light-matter-interacting system with two fundamentally distinct approaches:

(a) *Semiclassical approach.* To deal with the macroscopic number of atoms, we amend the quantum trajectory method with a semiclassical approximation using a stochastic photonic mean field. This approach is designed in a way such that the interaction of light with each individual atom is described in microscopic fashion, i.e., compatible with the constraints imposed by quantum information. However, the semiclassical approach assumes independent atoms and thus neglects possible (quantum) correlations between the atoms. As our approach is capable to describe time-integrated measurement statistics beyond the mean value, it complements the common treatment in light-matter interaction for uncorrelated quantum emitters based

on the Maxwell-Bloch equations [71, 72], which is abundantly used in spectroscopy [71] and optical magnetometers operating with optical thick vapors [19, 73–75].

(b) *Collective approach.* To circumvent the shortcomings of uncorrelated atoms, we investigate a collective model of the atomic ensemble in terms of collective spin operators. While this model strictly speaking does not reflect the experimental circumstances as it neglects local dissipation effects, it is theoretically consistent, crucial for a quantum-information-theoretic interpretation. Our approach generalizes the description of the probe light using Stokes operators and a local Bogoliubov approximation [32–35]: Here, the system is described in terms of a density matrix representation (amended with full-counting statistics) instead of the more common quantum Langevin equations, allowing for a straightforward investigation of the global parameter regime.

(ii) The second objective of this work is the analysis of optical magnetometry in terms of the Fisher information:

- (a) The semiclassical quantum information analysis shows that the quantum Cramer-Rao inequality [Eq. (1)], can be violated by the semiclassical description of the optical magnetometer, implying the invalidity of the semiclassical approach. This violation is shown in Fig. 1(c) for realistic experimental parameters. In principle, the Cramer-Rao bound can be violated by several orders of magnitude for an appropriate choice of parameters. This violation is especially prominent in the large atom-number regime and for a weak dissipation, suggesting to be induced by an emergent collective quantum effect. Implicitly assuming independent atoms, the semiclassical framework discards correlations between the atoms, which are indispensable for the validity of the quantum Cramer-Rao bound.
- (b) Crucially, by construction the collective approach strictly respects the Cramer-Rao bound, as shown in Fig. 1(d). As the model Hamiltonian does not contain any direct atom-atom interaction terms, the atomic correlations, indispensable for the Cramer-Rao-bound validity, must be thus induced by the measurement. As such, it constitutes a macroscopic nontrivial quantum state consisting of 10^{10} and more entities.

Interestingly, in the large-atom-number regime, the collective model predicts the Heisenberg scaling of the quantum Fisher information as a function of the atom number. In contrast to any interaction driven Heisenberg scaling [41–51], the comparison of the semiclassical and the collective treatment shows that the Heisenberg scaling are induced by the measurement itself, and seems to be inevitable in face of quantum information constraints. This is reminiscent of the preparation of optical clock atoms in an entangled state in an optical cavity by a dispersive measurement in Ref. [76]. Yet, as the collective magnetometer model investigated here predicts the Heisenberg scaling in a stationary state, it can be seen as a new paradigm in quantum sensing. Our findings thus suggest, that collective emission effects in spectroscopy similar to [77–79] can not only induce free-space Dicke superradiance, but also give rise to a quantum advantage in spectroscopic quantum sensing.

The rest of the paper is organized as follows: In Sec. II, we introduce the microscopic Hamiltonian of the optical magnetometer (Sec. II A) and carry out some fundamental quantum information considerations (Sec. II B). In Sec. III, we investigate two distinct magnetometer models: In Sec. III A, we introduce a semiclassical model assuming independent atoms, and in Sec. III B, we examine a collective model describing the atomic ensemble as a collective spin. Subsequently in Sec. III C, we interpret and compare the predictions of both models. In Sec. IV, we conclude and give an outlook to future work.

The main text of this article focuses on the physical aspects, while the theoretical foundations and the detailed derivations are provided in the appendices.

II. OPTICAL MAGNETOMETRY

A. Microscopic Hamiltonian

The experimental setup of a typical optical magnetometer is sketched in Fig. 1(a), where linearly-polarized laser light propagates through an atomic vapor [19]. The interaction with the atoms induces a rotation of the polarization direction, which is finally measured by a polarization beam splitter and two photon detectors. Typically, alkali atoms are being deployed due to their well-understood level structure and their long ground-state coherence times.

We model the system such that it fulfills basic physical constraints, in particular, the symmetry conditions which give rise to optical selection rules of the atomic transitions matrix elements. To this end, we describe the atoms by the Hamiltonian [26],

$$\hat{H} = \hat{H}_L + \sum_m \hat{H}_{M,m} + \sum_m \hat{H}_{LM,m}, \quad (2)$$

where \hat{H}_L denotes the Hamiltonian of the free radiation field. We model the relevant physical properties of the atoms as four-level systems sketched in Fig. 1(b), whose Hamiltonian is given by

$$\begin{aligned} \hat{H}_{M,m} = & \sum_{a=\pm 1} \epsilon |e_{m,a}\rangle \langle e_{m,a}| \\ & - \mu B_x (|g_{m,+}\rangle \langle g_{m,-}| + |g_{m,-}\rangle \langle g_{m,+}|) \\ & - \mu B_y i (|g_{m,+}\rangle \langle g_{m,-}| - |g_{m,-}\rangle \langle g_{m,+}|) \\ & - \mu B_z (|g_{m,+}\rangle \langle g_{m,+}| - |g_{m,-}\rangle \langle g_{m,-}|), \end{aligned} \quad (3)$$

where $m \in \{1, \dots, N\}$ labels the atom. The states $|g_{m,a}\rangle$ and $|e_{m,a}\rangle$ denote the ground and excited states of atom m , respectively. The index $a = \pm 1$ refers to the quantization of the atom in the z direction. Moreover, ϵ is the energy of the excited-state manifold. The atoms are subject to the magnetic field $\mathbf{B} = (B_x, B_y, B_z)$. The parameter μ denotes the magnetic moment of the ground-state manifold. In the following, we assume $B_y = 0$ for simplicity.

The light-matter interaction in Eq. (2) is given by the Hamiltonian

$$\begin{aligned} \hat{H}_{LM,m} = & d_A \sum_{a=\pm 1} \left[|e_{m,-a}\rangle \langle g_{m,a}| \hat{E}_x^{(-)}(\mathbf{r}_m) + \text{h.c.} \right] \\ & + d_A \sum_{a=\pm 1} \left[i |e_{m,-a}\rangle \langle g_{m,a}| \hat{E}_y^{(-)}(\mathbf{r}_m) + \text{h.c.} \right] \\ & + d_A \sum_{a=\pm 1} \left[|e_{m,a}\rangle \langle g_{m,a}| \hat{E}_z^{(-)}(\mathbf{r}_m) + \text{h.c.} \right], \end{aligned} \quad (4)$$

where the $\hat{E}_\eta(\mathbf{r})$ denotes the $\eta = \text{x}, \text{y}, \text{z}$ polarization-direction of the quantized electromagnetic field at position \mathbf{r} , and d_A is the transition dipole moment between the ground and excited-state manifold. Crucially, this modeling of the atom-light interaction respects optical selections rules.

B. Quantum information considerations

The Cramer-Rao bound imposes a fundamental limitation on the measurement sensitivity in terms of the Fisher information [39]. Here, we discuss a modified version of the quantum Cramer-Rao bound [80], which can be directly related to spectroscopic measurements.

To this end, we assume that solely the matter Hamiltonian $\hat{H}_M = \sum_m \hat{H}_{M,m}$ depends on the parameter of interest X , i.e., $\hat{H}_M = \hat{H}_{M,X}$. The generator of the quantum Fisher information is then given by $\hat{F}(t) = \partial_X \hat{H}_{M,X}(t)$, where the time evolution is determined by the Hamiltonian in Eq. (2). The quantum Fisher information can be calculated by

$$\mathcal{I}_X^{(Q)} = 4 \int_0^\tau dt_1 \int_0^\tau dt_2 \langle \Delta \hat{F}(t_1) \Delta \hat{F}(t_2) \rangle, \quad (5)$$

where $\Delta \hat{F}(t) = \hat{F}(t) - \langle \hat{F}(t) \rangle$, i.e., as the time-integrated noise of \hat{F} [81]. Here and in the following, $\langle \bullet \rangle$ refers to the expectation value in the initial state of the system.

The quantum Fisher information equals the signal-to-noise ratio \mathcal{S}_A maximized over all measurement operators \hat{A} [80], i.e.,

$$\mathcal{I}_X^{(Q)} = \max_{\hat{A}} \mathcal{S}_X^{(A)}, \quad \text{where} \quad \mathcal{S}_X^{(A)} \equiv \frac{\langle \partial_X \hat{A}(\tau) \rangle^2}{\langle \Delta \hat{A}^2(\tau) \rangle}, \quad (6)$$

where $\Delta \hat{A} = \hat{A} - \langle \hat{A} \rangle$. We will refer to $\partial_X \hat{A}(\tau)$ as the signal operator. For completeness, this relation is also shown in Appendix A 1 for Hamiltonian parameter estimation using a linear-response theory approach. By setting $\hat{X} = \Delta \hat{A} / \langle \partial_X \hat{A}(\tau) \rangle$ in Eq. (1), the relation to Eq. (6) is evident.

Crucially, this relation also holds for all spectroscopic observables, which typically record the intensity of light as a function of time. Upon postprocessing of the measurement data, one can construct arbitrary measurement statistics, such as the time-integrated intensities

$$\hat{n}_\eta = \frac{\mathcal{A}}{\hbar \omega_p} \int_0^\tau \hat{\mathcal{J}}_\eta(t) dt, \quad (7)$$

where $\eta = \{\text{x}, \text{y}\}$ refers to the polarization direction and \mathcal{A} is the effective cross section of the laser. The intensities $\hat{\mathcal{J}}_\eta(t)$ in direction η can be measured using the polarization beam splitter and the two photon detectors in

Fig. 1(a). The time-integrated intensities are here expressed in units of photon numbers. Optical magnetometry considers the photon-number difference

$$\hat{n}_\eta = \hat{n}_x - \hat{n}_y \quad (8)$$

as measurement operator (i.e., $\hat{A} = \hat{n}_\eta$), whose statistics sensitively depends on B_z via the Faraday effect [19, 74].

Now we make some considerations regarding the many-body character of optical magnetometry. Defining the generator of the Fisher information of atom m as $F_m(t) = \partial_X \hat{H}_{M,m,X_0}(t)$, the Fisher information in Eq. (5) can be expressed as

$$\mathcal{I}_X^{(Q)} = 4 \int_0^\tau dt_1 \int_0^\tau dt_2 \sum_{m_1, m_2} \langle \Delta \hat{F}_{m_1}(t_1) \Delta \hat{F}_{m_2}(t_2) \rangle, \quad (9)$$

where $\Delta \hat{F}_m(t) = \hat{F}_m(t) - \langle \hat{F}_m(t) \rangle$. This representation already hints a major obstacle of a semiclassical description. Semiclassically, the atoms are regarded as independent, such that correlations between distinct atoms $m_1 \neq m_2$ are discarded [10]. However, as the evaluation of the optical magnetometer in Sec. III A showcases, such a semiclassical approach can lead to a drastic violation of the Cramer-Rao inequality. This shows the insufficiency of the semiclassical approach in spectroscopy and the demand for a collective description of the atomic ensemble.

III. MODEL ANALYSIS

In this section, we will deploy two distinct approaches to describe the interaction of the light field with the atomic ensemble in an optical magnetometer. First, we investigate a semiclassical approach, in which we assume that each atom interacts independently with the light field in Sec. III A. After showing the insufficiency of this approach with regard to quantum information, we consider a collective description of the atomic ensemble, which complies with the Cramer-Rao bound in Sec. III B.

To allow for physically meaningful interpretations, we use the following experimentally reasonable parameters unless stated differently. Taking the D₂ transition in ⁸⁵Rb as reference, we assume an electronic dipole moment of $d_A = 4.23ea_0$ (elementary charge e , Bohr radius a_0). The probe laser, propagating in the positive z direction, has wavelength $\lambda = 780$ nm and is detuned from the excited state manifold by $\epsilon_\Delta = \epsilon - \omega_p = 10$ GHz. The excited state manifold exhibits a decay rate $\gamma = 6$ MHz. The magnetic field in x direction gives rise to a Lamor frequency of $\mu B_x / \hbar = 500$ kHz. The probe laser is assumed to have power $P_p = 10 \mu\text{W}$ and waist $w_p = 200 \mu\text{m}$. This gives rise to a Rabi frequency of $\Omega = d_A E_p / \hbar = 25$ MHz. The atomic ensemble has a length of $l = 2$ cm. Atomic densities are assumed to be in the range $\rho_A = 10^{10} \text{ cm}^{-3} - 10^{16} \text{ cm}^{-3}$ [82, 83], corresponding to about $N = 10^7$ till $N = 10^{13}$ atoms

effectively participating in the light-matter interaction. Moreover, we assume an effective pump of $\gamma_P = 30$ kHz which magnetically polarizes the atoms in the positive x direction. The mean photon number emitted by the laser over the measurement duration of $\tau = 1$ s is $\bar{n}_+^{(i)} = 6 \cdot 10^{12}$.

A. Semiclassical model

Within the semiclassical approach, the light-matter interaction for a single atom is assumed to be independent of the other atoms. In Appendix B 2, we deploy a Markovian quantum-trajectory method to derive a master equation, which guarantees microscopic consistency of quantum information constraints for the light-matter interaction of each individual atom. In the large detuning regime $\epsilon - \omega_P \gg \gamma$, the master equation of a single atom can be adiabatically projected to the ground-state manifold, which eventually reads

$$\begin{aligned} \frac{d}{dt}\rho = & -i\frac{\mu}{2}[B_x\hat{\sigma}_x + B_z\hat{\sigma}_z, \rho] \\ & + \frac{\Gamma\Omega^2}{\epsilon_\Delta^2 + \frac{\Gamma^2}{4}} \sum_{a=\pm 1} D[\hat{\pi}_a]\rho + \gamma_P D\left[\frac{1}{2}(\hat{\sigma}_z - i\hat{\sigma}_y)\right]\rho, \end{aligned} \quad (10)$$

where $\hat{\sigma}_\alpha$ with $\alpha \in \{x,y,z\}$ are the standard Pauli spin matrices in the basis of $|g_{-1}\rangle, |g_{+1}\rangle$ and $\hat{\pi}_a = (\hat{1} + a\hat{\sigma}_z)/2$ are projectors on the $a = \pm 1$ eigenstates in the z basis. Thereby, we have also phenomenologically introduced a pumping term proportional to γ_P , and

$$D[\hat{O}]\rho = \hat{O}\rho\hat{O}^\dagger - \frac{1}{2}\{\hat{O}^\dagger\hat{O}, \rho\} \quad (11)$$

is the common dissipator. This additional pump term does not impact the validity of the Cramer-Rao bound in Eq. (1). The effective decay rate $\Gamma = \gamma + \gamma_z$ is a sum of the spontaneous decay rate in an arbitrary direction γ , and the decay rate in the direction of the probe-beam direction γ_z . The latter appears within the quantum-trajectory approach and strictly fulfills $\Omega = 2\sqrt{\gamma_z\bar{n}_+/\tau}$. While it can be neglected in the semiclassical approach as $\gamma_z \ll \gamma$, this parameter plays a crucial role in the collective model due to distinct scaling properties (see Sec. III B).

The expectation values for the spin operators are depicted in Fig. 2(a). The quantum Fisher information can be evaluated using Eq. (9) with $\hat{F}_{B_z,m} = \mu\hat{\sigma}_z/2$. Within the semiclassical approach, we thereby neglect terms with $m_1 \neq m_2$.

An optical magnetometer determines the rotation of the linearly polarized laser light $\bar{\theta}$ by measuring the difference of the photon numbers in the x and y direction defined in Eq. (8). Within the semiclassical approach, the propagation of the probe light through the atomic vapor is described by a Maxwell-Bloch equation as shown in

Appendix C. In doing so, we find that

$$\langle \hat{n}_-(\tau) \rangle = \bar{n}_+^{(f)} \sin(2\bar{\theta}), \quad (12)$$

where $\bar{n}_+^{(f)} = e^{-\check{I}_+ N} \bar{n}_+^{(i)}$ denotes the total number of the recorded photons after having interacted with N atoms, when the initial total photon number is $\bar{n}_+^{(i)}$. The polarization rotation due to the light-matter interaction can be expressed by $\bar{\theta} = \check{I}_- N$. Thereby,

$$\check{I}_\pm = \frac{1}{\bar{n}_+(0)} \int_0^\tau \langle \hat{j}_\pm(t) \rangle dt \quad (13)$$

with $\hat{j}_\pm = \hat{j}_x \pm \hat{j}_y$ and

$$\begin{aligned} \hat{j}_x\rho = & \frac{\Omega^2}{2} \left\{ \left[\frac{1+i}{\epsilon_\Delta - i\frac{\Gamma}{2}} \hat{\pi}_1 + \frac{-1+i}{\epsilon_\Delta - i\frac{\Gamma}{2}} \hat{\pi}_{-1} \right] \rho + \text{h.c.} \right\} \\ & + \frac{\gamma_z\Omega^2}{\epsilon_\Delta^2 + \frac{\Gamma^2}{4}} \{ \hat{\pi}_1\rho\hat{\pi}_1 + \hat{\pi}_{-1}\rho\hat{\pi}_{-1} \}, \\ \hat{j}_y\rho = & \frac{\Omega^2}{2} \left\{ \left[\frac{-1+i}{\epsilon_\Delta - i\frac{\Gamma}{2}} \hat{\pi}_1 + \frac{1+i}{\epsilon_\Delta - i\frac{\Gamma}{2}} \hat{\pi}_{-1} \right] \rho + \text{h.c.} \right\} \\ & + \frac{\gamma_z\Omega^2}{\epsilon_\Delta^2 + \frac{\Gamma^2}{4}} \{ \hat{\pi}_1\rho\hat{\pi}_1 + \hat{\pi}_{-1}\rho\hat{\pi}_{-1} \}, \end{aligned} \quad (14)$$

which can be evaluated by integrating Eq. (10). Noteworthy, the operator $\partial_{B_z} H_{M,m} = \mu\hat{\sigma}_z/2$ is proportional to \hat{j}_- for a vanishing dissipation Γ , such that the noise of $\hat{n}_-(\tau)$ is closely related to the Fisher information in the adiabatic ground-state approximation of the four-level system.

To optimize the sensitivity, typically one measures in a measurement basis rotated by $\bar{\theta}$ such that the average number of photons in each polarization direction is equal, i.e., $\langle \hat{n}_{\text{rot},-}(\tau) \rangle = 0$ for a particular reference magnetic field $B_z^{(0)}$. In this basis, we find

$$\langle \partial_{B_z} \hat{n}_{\text{rot},-}(\tau) \rangle = \bar{n}_+^{(f)} N \frac{d\check{I}_-}{dB_z}. \quad (15)$$

The corresponding noise can be obtained on an equal footing and reads

$$\langle \Delta\hat{n}_{\text{rot},-}^2(\tau) \rangle = N\mathcal{D} + \bar{n}_+^{(f)}, \quad (16)$$

where $\bar{n}_+^{(f)}$ is the photon-shot-noise and

$$\mathcal{D} = \int_0^\tau dt_1 \int_0^\tau dt_2 \langle \Delta\hat{j}_-(t_1)\Delta\hat{j}_-(t_2) \rangle \quad (17)$$

with $\Delta\hat{j}_-(t) = \hat{j}_-(t) - \langle \hat{j}_-(t) \rangle$ can be interpreted as a diffusion parameter. The latter can be efficiently evaluated using a full-counting statistics approach as shown in Appendix B 2.

The master equation in Eq. (10) allows for an analyti-

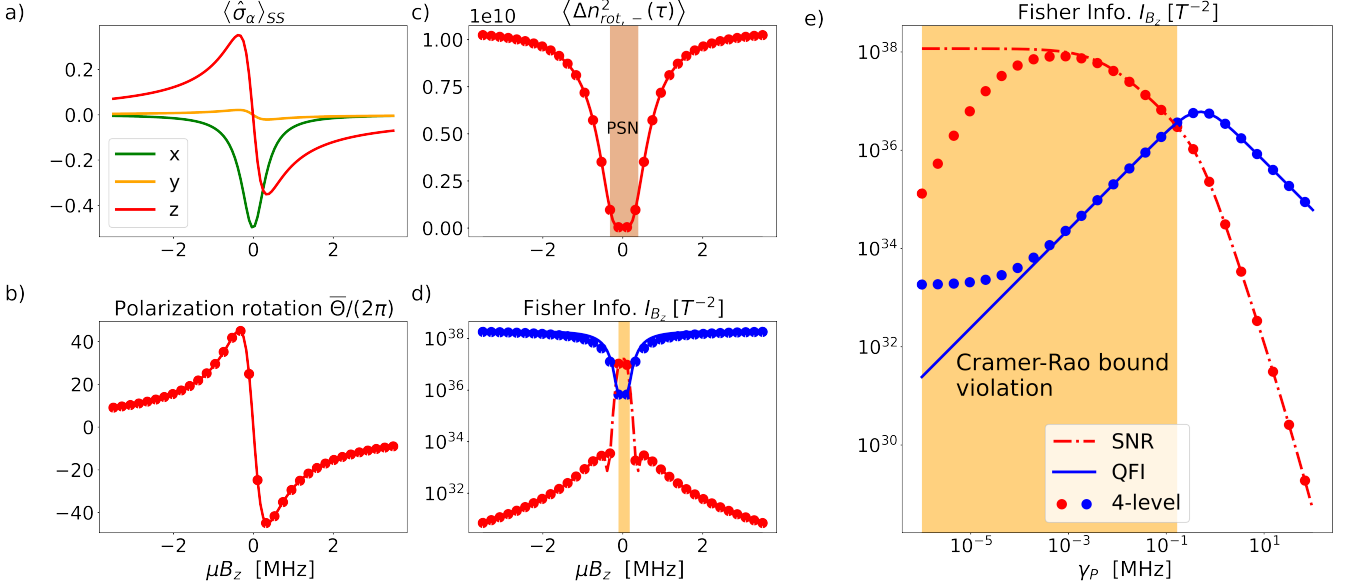


FIG. 2. Investigation of the semiclassical model. (a) Expectation value of the spin operators as a function of B_z in the stationary state of the master equation in Eq. (10). (b) Expectation value of the polarization rotation in Eq. (18). (c) Variance of $\hat{A}_{\text{rot}}(\tau)$ as given in Eq. (20). (d) The quantum Fisher information [QFI, blue, expression below Eq. (20)] exceeds the signal-to-noise ratio [SNR, red, Eq. (20)] for almost all B_z except for $|B_z| \approx 0$, where the Cramer-Rao bound is violated. (e) The violation becomes more pronounced in the weak pump regime. The colored curves depict the results in the ground-state manifold master equation in (10), while the black (dashed) line shows the calculation using the master equation for the four-level system for validation. Overall parameters are explained in Sec. III, and $N = 8 \cdot 10^{10}$ atoms.

cal evaluation of Eqs. (12) and (16) for small dissipation Γ and large detuning ϵ_Δ . Introducing $h_\alpha = \mu B_\alpha$ for brevity, we obtain

$$\bar{\theta} = \frac{\tau}{\bar{n}_+^{(i)}} \frac{N \mathcal{C}_A 32 h_x h_z}{2 h_z^2 + 4 h_x^2 + \gamma_P^2}, \quad (18)$$

where N is the number of atoms involved in the light-matter interaction, and $\mathcal{C}_A = \Omega^2/\epsilon_\Delta$. Consequently the derivative in the rotated measurement basis is given by

$$\begin{aligned} \langle \partial_{B_z} \hat{n}_{\text{rot},-}(\tau) \rangle &= \frac{\tau N \mathcal{C}_A 32 h_x \mu}{2 h_z^2 + 4 h_x^2 + \gamma_P^2} \\ &+ \frac{\tau N \mathcal{C}_A 64 h_x h_z^2 \mu}{(2 h_z^2 + 4 h_x^2 + \gamma_P^2)^2}. \end{aligned} \quad (19)$$

Evaluation of Eq. (16) yields

$$\begin{aligned} \langle \Delta \hat{n}_{\text{rot},-}^2(\tau) \rangle &= \bar{n}_+^{(f)} + \tau N \mathcal{C}_A^2 \frac{32 h_z^2 + 4 \gamma_P^2}{2 \gamma_P h_z^2 + 4 \gamma_P h_x^2 + \gamma_P^3} \\ &- 2 \tau N \mathcal{C}_A^2 \frac{(4 h_z^2 + 4 h_x^2 + \frac{5}{4} \gamma_P^2) (8 \gamma_P h_x h_z)^2}{(2 \gamma_P h_z^2 + 4 \gamma_P h_x^2 + \gamma_P^3)^3}, \end{aligned} \quad (20)$$

Moreover, within the adiabatic approach employed here, we find $\mathcal{I}_{B_z}^{(Q)} = \mu^2 \left(\langle \Delta \hat{n}_{\text{rot},-}^2(\tau) \rangle - \bar{n}_+^{(i)} \right) / \mathcal{C}_A^2$. This inti-

mate relation is a consequence of $\dot{j}_- \propto \partial_{B_z} \hat{H}_M$ for optical magnetometers in the large detuning regime.

In Fig. 2, we depict the dependence of these quantities as a function of the magnetic field μB_z by colored lines. To demonstrate the accuracy of the adiabatic approach, we also depict these quantities for a non-adiabatic evaluation using the full four-level system in Eq. (2) (while still invoking the semiclassical approach).

In Fig. 2 (b), the polarization rotation $\bar{\theta}$ abides to the well-known dispersion relation, reflecting the relation between the refractive index and the Faraday effect. In Fig. 2 (c), we depict the variance $\langle \Delta \hat{n}_{\text{rot},-}^2(\tau) \rangle$ in the rotated measurement frame. In the vicinity of $B_z \approx 0$ the variance exhibits a flat minimum, where the minimal value is given by the photon-shot noise. For large $|B_z|$, the variance increases drastically and is dominated by the second and third terms in Eq. (20), which scale in the weak pumping regime with $1/\gamma_P$. This behavior is a consequence of probabilistic jumps between the eigenstates [10, 84].

To analyze the information content in this setup, we depict the quantum Fisher information $\mathcal{I}_{B_z}^{(Q)}$ and the signal-to-noise ratio $\mathcal{S}_{B_z}^{(n_{\text{rot},-})}$ of the integrated polarization measurement in Fig. 2(d). For large $|B_z| \gg 0$, we find that $\mathcal{I}_{B_z}^{(Q)}$ exceeds $\mathcal{S}_{B_z}^{(n_{\text{rot},-})}$ by several orders of magnitude. This is to be expected as a considerable amount of information is lost by the temporal average in Eq. (7). The strongly suppressed signal-to-noise ratio results from

large noise induced by the light-matter interaction. The weak dissipation gives rise to positively-correlated fluctuations in time, which detrimentally influence the signal-to-noise ratio [10, 85].

Surprisingly, for $|B_z| \approx 0$, we observe $\mathcal{I}_{B_z}^{(Q)} < \mathcal{S}_{B_z}^{(n_{\text{rot}}, -)}$, meaning that the Cramer-Rao inequality is violated. To further investigate this, we depict both quantities in Fig. 1(c) as a function of the atom number. For benchmarking, we also add the calculation for the four-level model. We observe that the quantum Fisher information increases linearly with the atom number as predicted by the analytical calculation. For small atom numbers, the signal-to-noise ratio increases quadratically with the atom number. In this regime, the noise is dominated by the photon-shot noise, which is independent of the atom number, while the signal in Eq. (19) scales linearly with N . Above $N \approx 10^8$ we observe that $\mathcal{I}_{B_z}^{(Q)} < \mathcal{S}_{B_z}^{(n_{\text{rot}}, -)}$, i.e, the Cramer-Rao inequality is violated almost two orders of magnitude. For even larger N , $\mathcal{S}_{B_z}^{(n_{\text{rot}}, -)}$ becomes flatter and eventually decreases. In this regime, the absorption becomes significant, leading to an exponential suppression of the signal with the atom number.

To better understand the occurrence of the semiclassical Cramer-Rao bound violation, we evaluate $\mathcal{S}_{B_z}^{(n_{\text{rot}}, -)}$ in Eq. (1) in the limit $N \rightarrow \infty$, and compare it to the quantum Fisher information. Their ratio becomes

$$\frac{\mathcal{S}_{B_z}^{(n_{\text{rot}}, -)}}{\mathcal{I}_{B_z}^{(Q)}} \rightarrow \frac{\mu B_x}{\gamma_P}, \quad (21)$$

implying that the Cramer-Rao bound is possibly violated for $\mu B_x > \gamma_P$. To investigate this assertion quantitatively, we depict the Fisher information and the signal-to-noise ratio as a function of the pump γ_P in Fig. 2(e). For the two-level system (depicted by colored lines), the Cramer-Rao inequality is violated by several orders of magnitude in the weak pumping regime. This is also confirmed by the four-level system calculation. Only in the very weak pump regime for which $\gamma_P < \Gamma\Omega^2/\epsilon_\Delta^2$, we observe significant deviations between the two- and the four-level-system calculations, as there the dissipative dynamics is dominated by excited-state processes.

The analysis thus demonstrates that a semiclassical Cramer-Rao bound violation is possible for large atom numbers and for weak dissipation. This suggests an emergent collective quantum effect, which is not captured by the semiclassical approach assuming independent atoms. These collective dynamics eventually gives rise to additional contributions to the quantum Fisher information required to restore the Cramer-Rao bound, i.e., the terms with $m_1 \neq m_2$ in Eq. (9).

B. Collective model

The insufficiency of the semiclassical approach suggests to describe the atomic ensemble in a collective manner

which allows to consistently account for the correlation functions terms with $m_1 \neq m_2$ in Eq. (9). To this end, we assume that the atoms are indistinguishable with respect to the light-matter interaction. Physically, this corresponds to a situation where all atoms are located at the same position $\mathbf{r}_m = \mathbf{r}_0$.

As for the semiclassical treatment in Sec. III A, we project the dynamics onto the ground-state manifold within an adiabatic approximation. Introducing the collective atomic operators $\hat{S}_{a,b} = \sum_{m=1}^N |g_{m,a}\rangle \langle g_{m,b}|$, we can define the collective spin operators as

$$\begin{aligned} \hat{S}_x &= \frac{1}{2} (\hat{S}_{1,-1} + \hat{S}_{-1,1}), \\ \hat{S}_y &= \frac{i}{2} (\hat{S}_{1,-1} - \hat{S}_{-1,1}), \\ \hat{S}_z &= \frac{1}{2} (\hat{S}_{1,1} - \hat{S}_{-1,-1}). \end{aligned} \quad (22)$$

In terms of these, the master equation for the reduced density matrix of the collective ground-state manifold reads

$$\begin{aligned} \frac{d}{dt} \rho &= -i\mu [B_x \hat{S}_x + B_z \hat{S}_z, \rho] \\ &+ \frac{\Gamma\Omega^2}{\epsilon_\Delta^2 + \frac{\Gamma^2}{4}} \sum_{a=\pm 1} D[\hat{P}_a] \rho + \gamma_P D[\hat{S}_z - i\hat{S}_y] \rho, \end{aligned} \quad (23)$$

where $\hat{P}_{\pm 1} = \hat{S}_{\pm 1, \pm 1}$ is a collective operator counting the atoms in state ± 1 . Notably, the collective master equation is formally equivalent to the semiclassical master equation in Eq. (10). As in Sec. III A, $\Gamma = \gamma + \gamma_z$. In the following, we investigate the system as a function of $\tilde{\gamma}$ and $\tilde{\gamma}_P$ such that $\gamma = \tilde{\gamma}/N$ and $\gamma_P = \kappa_P/N$. In doing so, we obtain a well-defined semiclassical limit $N \rightarrow \infty$ for the ground-state manifold, allowing for a straightforward comparison with the semiclassical model. However, such a rescaling is not feasible for the dissipation resulting from the excited-states, which has to strictly fulfill $\Omega = 2\sqrt{\gamma_z \bar{n}_+/\tau}$ to ensure a microscopically consistent master equation to fulfill the Cramer-Rao bound [see Eq. (B20)]. Crucially, the master equation (23) generalizes the description of the light-matter interaction in terms of the collective Stokes operators and Bogoliubov transformation, which is typically deployed to investigate quantum precision limits of atomic interferometers [32–35, 62, 64]. Here, we consider the system on the ensemble level instead of the more common quantum Langevin equations, allowing to conveniently investigate the global quantum information content of the system.

The expectation values $\langle \hat{S}_\alpha \rangle / N$ for $\alpha = \{x, y, z\}$ in the stationary state evaluated in the thermodynamics limit $N \rightarrow \infty$ are depicted in Fig. 3(a). Interestingly, the expectation values for $\alpha = x, y$ closely resemble the ones in the semiclassical description in Fig. 2(a). This is also true for $\alpha = z$ around $|B_z| \approx 0$. Yet, for increasing $|B_z|$

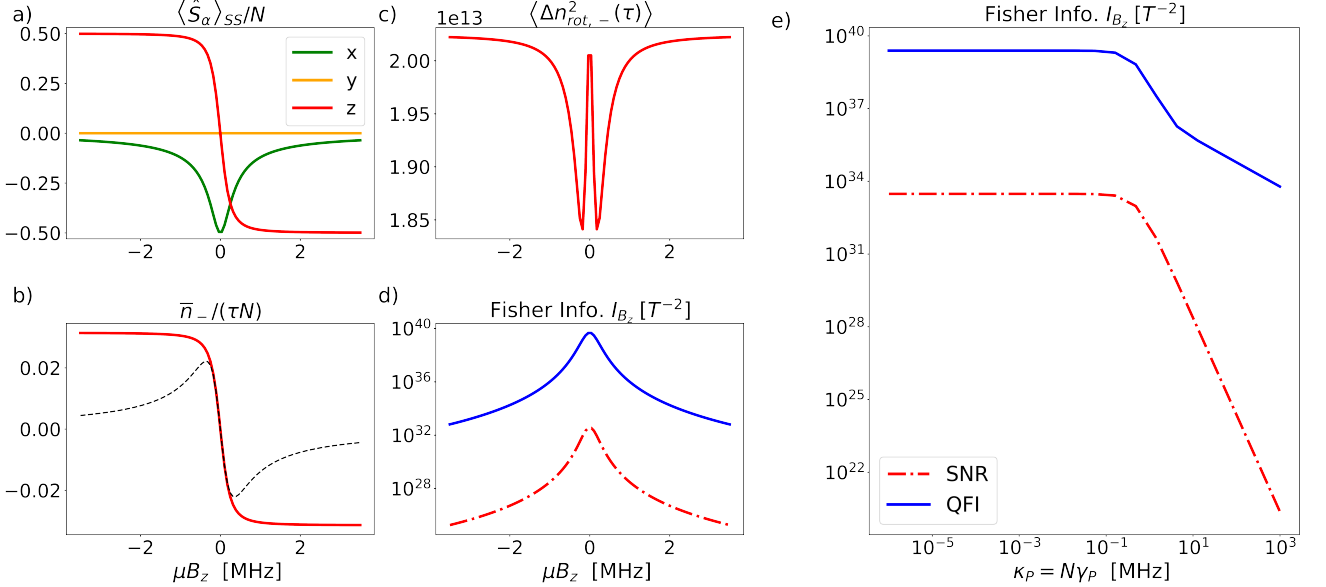


FIG. 3. Investigation of the collective model. (a) Expectation value of the spin operators as a function of B_z in the stationary state of the master equation in Eq. (23). (b) Expectation value of the measured mean photon number difference Eq. (26). The scaling by τN allows us to compare it to the scaled polarization rotation depicted by the black dashed line (c) Variance of $\hat{n}_{\text{rot},-}(\tau)$ defined in Eq. (28). (d) The quantum Fisher information [QFI, blue] exceeds the signal-to-noise ratio [SNR, red] everywhere, such that the Cramer-Rao bound is respected. (e) The Cramer-Rao bound is maintained in all pump regimes due to the microscopic derivation of the master equation. Overall parameters are explained in Sec. III. We consider $N = 8 \cdot 10^{10}$ and a scaled $\gamma_P = 30\text{kHz}/N$ to mimic a non-collective pump.

the collective expectation value approaches ± 1 , while the one of the semiclassical description gradually vanishes. This is a consequence of the pump term $\propto \gamma_P$: In the semiclassical description, a pump-term-induced spin flip completely inverts the polarization direction of the atom. For the collective model, a single pump event has only a minor impact on the direction of the collective spin polarization. This stability allows the collective spin to reach larger values for the polarization in the z direction.

Moreover, we obtain the quantum Fisher information by evaluating Eq. (5) with $\partial_{B_z} \hat{H}_M = \mu \hat{S}_z$. In Appendix E 2, we introduce a method to evaluate integrated two-point correlation functions of collective spin systems in the thermodynamics limit $N \rightarrow \infty$ using a non-unitary mean-field transformation amended with methods of full-countings statistics.

To predict the measurement statistics, we introduce the effective photonic intensity operators

$$\begin{aligned} \hat{\mathcal{J}}_x \rho &= \frac{\Omega^2}{2} \left\{ \left[\frac{1+i}{\epsilon_\Delta - i \frac{\Gamma}{2}} \hat{P}_1 + \frac{-1+i}{\epsilon_\Delta - i \frac{\Gamma}{2}} \hat{P}_{-1} \right] \rho + \text{h.c.} \right\} \\ &+ \frac{\gamma_z \Omega^2}{\epsilon_\Delta^2 + \frac{\Gamma^2}{4}} \left\{ \hat{P}_1 \rho \hat{P}_1 + \hat{P}_{-1} \rho \hat{P}_{-1} \right\} + \hat{\mathcal{J}}_x^{(0)} \rho, \\ \hat{\mathcal{J}}_y \rho &= \frac{\Omega^2}{2} \left\{ \left[\frac{-1+i}{\epsilon_\Delta - i \frac{\Gamma}{2}} \hat{P}_1 + \frac{1+i}{\epsilon_\Delta - i \frac{\Gamma}{2}} \hat{P}_{-1} \right] \rho + \text{h.c.} \right\} \end{aligned}$$

$$+ \frac{\gamma_z \Omega^2}{\epsilon_\Delta^2 + \frac{\Gamma^2}{4}} \left\{ \hat{P}_1 \rho \hat{P}_1 + \hat{P}_{-1} \rho \hat{P}_{-1} \right\} + \hat{\mathcal{J}}_y^{(0)} \rho, \quad (24)$$

which act on the ground-state manifold. The operators $\hat{\mathcal{J}}_x^{(0)}, \hat{\mathcal{J}}_y^{(0)}$ describe the Poisson statistics of the incoming photonic fields in x and y directions. In terms of the operators, the time-integrated intensity average in each direction is given by

$$\bar{n}_{x/y} = \int_0^\tau \left\langle \hat{\mathcal{J}}_{x/y}(t) \right\rangle dt, \quad (25)$$

in units of the photon number. Using these quantities, we can calculate the mean difference for the measurements in x and y directions via

$$\bar{n}_- = \bar{n}_x - \bar{n}_y, \quad (26)$$

and likewise $\bar{n}_+ = \bar{n}_x + \bar{n}_y$. Due to the collective nature of the model, it is not possible to describe a rotation of the light polarization by more than $|\bar{\theta}| = \pi/2$. To nevertheless compare \bar{n}_- with the rotation angle $\bar{\theta}$ in the semiclassical model, we will consider the scaled quantities $\bar{n}_-/(\bar{n}_+ N)$ and $\bar{\theta}/N$.

As in Sec. III A, we are going to measure the system in a rotated measurement basis, in which the photon-number difference of the two polarization directions vanishes. To this end, we introduce the weighted operators

$\hat{J}_{\text{rot},\pm} = c_x \hat{J}_x \pm c_y \hat{J}_y$ for which

$$\langle \hat{n}_{\text{rot},-}(\tau) \rangle = \int_0^\tau dt \langle \hat{J}_{\text{rot},-}(t) \rangle \quad (27)$$

vanishes, and the total photon number remains unchanged. Within the microscopic quantum trajectory approach, the noise of $\hat{n}_{\text{rot},-}$ is given by

$$\begin{aligned} \langle \Delta \hat{n}_{\text{rot},-}^2(\tau) \rangle &= \int_0^\tau dt \langle \hat{J}_{\text{rot},+}(t) \rangle \\ &+ \int_0^\tau dt_1 \int_0^\tau dt_2 \langle \Delta \hat{J}_{\text{rot},-}(t_1) \Delta \hat{J}_{\text{rot},-}(t_2) \rangle, \end{aligned} \quad (28)$$

where $\Delta \hat{J}_{\text{rot},-}(t) = \hat{J}_{\text{rot},-}(t) - \langle \hat{J}_{\text{rot},-}(t) \rangle$. Of note, within the adiabatic approximation used to derive the master equation in Eq. (23), the first term in Eq. (28) exactly vanishes, as formally the excited-state manifold is only virtually excited. The second term in Eq. (28) can be efficiently evaluated using the non-unitary mean field theory introduced in Appendix E2, which analyzes the equation of motions Eq. (23) in the leading order of the atom number, that is, the thermodynamic limit $N \rightarrow \infty$.

In Fig. 3, we analyze these quantities as a function of B_z . Figure 3(b) depicts the scaled \bar{n}_- , whose functional form is almost indistinguishable from the \hat{S}_z expectation value in Fig. 3(a). For comparison, we also depict the scaled rotation angle of the semiclassical model $\bar{\theta}/N$ (dashed line). Interestingly, we find that both quantities agree to each other around $|B_z| \approx 0$. Thus, the semiclassical and the collective models make the same predictions for expectation values in this regime.

The corresponding measurement noise is shown in Fig. 3(c). Interestingly, it resembles the noise for the semiclassical approach shown in Fig. 3(c), Yet, it features a narrow peak within the central dip around $B_z = 0$. More importantly, the overall noise for all $|B_z|$ is three orders of magnitudes larger than for the semiclassical description, which is a consequence of the collective character of the dissipation in Eq. (23). It allows for the generation of correlations between the atoms, which overall increase the noise.

In Fig. 3(d), we analyze the quantum Fisher information $\mathcal{I}_{B_z}^{(Q)}$ and the signal-to-noise ratio $\mathcal{S}_{B_z}^{(n_{\text{rot},-})}$. The shape of $\mathcal{S}_{B_z}^{(n_{\text{rot},-})}$ is reminiscent of the one in the semiclassical description, except for the sharp decrease around $\mu B_z = \pm 0.25$ MHz, which is a consequence of the two extrema in Fig. 2(b). Intriguingly, the quantum Fisher information in the collective model is different from its semiclassical counterpart in Fig. 3(d). In particular, the collective description predicts a maxima in the quantum Fisher information at $B_z = 0$, ensuring the validity of the Cramer-Rao bound.

To investigate the collective nature, we depict $\mathcal{I}_{B_z}^{(Q)}$ and $\mathcal{S}_{B_z}^{(n_{\text{rot},-})}$ as a function of the atom number for $B_z = 0$ in

Fig. 1(d). Using the methods outlined in Appendix E3, we find that

$$\begin{aligned} \frac{\mathcal{I}_{B_z}^{(Q)}}{\tau \mu^2} &= N \frac{\kappa_P}{h_x^2 + \frac{\kappa_P^2}{4}} \left(\frac{\kappa_z}{2\kappa_P} + 1 \right) \\ &+ N \kappa_z \frac{h_x^2 - \frac{\kappa_P^2}{4}}{\left(h_x^2 + \frac{\kappa_P^2}{4} \right)^2}, \end{aligned} \quad (29)$$

where $h_x = \mu B_x$, and $\kappa_z = N \gamma_z \Omega^2 / \epsilon_\Delta^2$. For small N , the quantum Fisher information increases linearly. In this regime, the Fisher information leaks through the pumping action $\propto \kappa_P$ to the environment. The signal-to-noise ratio increases quadratically, as in this regime the measurement noise is dominated by the photon-shot noise. Once the atom number exceeds $N \approx 10^{10}$, the behavior changes. Now $\mathcal{I}_{B_z}^{(Q)}$ increases quadratically, i.e., it exhibits Heisenberg scaling. From this scaling, we conclude that the Fisher information leaks via the collective dissipation $\propto \gamma_z N$, which acts collectively on the atomic cloud in Eq. (23), hence the quadratic scaling with atom number. However, the signal-to-noise ratio becomes constant. In this regime, the increasing dissipation $\propto \gamma_z N$ progressively destroys the coherent dynamics of the spin system, required for the coherent rotation of the light polarization. Of note, the linear in τ scaling of Eq. (29) derived here on a microscopic footing invalidates the τ^3 scaling in Refs. [61, 62] derived under a Gaussian assumption.

Finally, we investigate the Fisher information as a function of the pump κ_P in Fig. 3(e). We find that the quantum Fisher information always exceeds the signal-to-noise ratio of the cumulative statistics, reflecting the microscopic consistency of the light-matter interaction in the collective model.

C. Discussion

The analysis of the optical magnetometer in terms of the two fundamentally different models merits a thorough discussion:

- *Physical interpretation.* The semiclassical violation of the quantum Cramer-Rao bound is a consequence of the neglected atomic correlations in the semiclassical description. As these correlations are accounted for in the collective description, the Cramer-Rao bound validity is reestablished. As a consequence, the quantum Fisher information in the semiclassical and the collective models are very distinct, while the mean values of observables exhibit a clear resemblance.

The semiclassical model neglects the quantum dynamics of the photonic field, which can become correlated with the atomic ensemble in a quantum description. When measured at the detector, the state collapses into the respective subspace of the

atomic ensemble. This state collapse generates correlations between the atoms. A similar effect has been observed for optical clock transitions in a cavity [76] and a hot-interacting atomic vapor [86], but our investigation suggests that it also prevails in a free space stationary state. To model the collective character of the magnetometer, we assumed that all atoms are located at the same position to enable a theoretical investigation. However, the fundamental reason for the correlation generation is the indistinguishability of the atoms with regard to the light-matter interaction: Once measured at the detector, a photon cannot recall with which atom it has interacted. Thus, even if the atoms are far apart from each other along the z direction, correlations *at a distance* will be induced by the measurement. This also implies that the buildup of correlations depends on the total atom number and not the density.

Heisenberg scaling of the quantum Fisher information has been predicted in several contexts. In the existing literature, interaction between sensing entities are necessary either for the state preparation or during the sensing phase [41–51]. The Heisenberg scaling as predicted in our investigation in the large atom-number regime is thereby outstanding, as it relies on measurement-induced correlations in a stationary state of the system. The fact that the process is induced by the dissipation itself suggests that it may be robust against environmental influences. Thus, as the semiclassical description is invalid, the Heisenberg scaling follows as an inevitable consequence.

- *Experimental distinction.* The analysis of both models suggests that the time-integrated intensity and its noise can distinguish the nature of the atomic correlations. According to the semiclassical calculation shown in Fig. 2(b), the polarization rotation will vanish for large $|B_z|$, while it will reach a plateau for the collective description in Fig. 3(b). Strikingly, the measurement noise predicted by the collective model in Fig. 3(c) drastically exceeds the prediction of the semiclassical ensemble description in Fig. 2(b). Furthermore, the present investigation is restricted to time-integrated observables. A more detailed analysis of the time-resolved measurement statistics can offer a host of information uncovering the nature of the correlations.

Interestingly, the validity of the Cramer-Rao bound can also be directly tested. A careful comparison of the measurement noise [Eq. (16) for the semiclassical model and Eq. (28) for the collective model] and the Fisher information [Eq. (5) for the semiclassical model and Eq. (9) for the collective model] shows that $\mu^2 \epsilon_{\Delta}^2 \langle \Delta \hat{n}_-^2(\tau) \rangle > \Omega^4 \mathcal{I}_{B_z}^{(Q)}$ in both models. For this reason, we can rephrase the Cramer-Rao bound

in Eq. (6) as

$$\frac{\mu^2 \epsilon_{\Delta}^2}{\Omega^4} \langle \Delta \hat{n}_-^2(\tau) \rangle > \langle \partial_{B_z} \hat{n}_-(\tau) \rangle^2, \quad (30)$$

which constitutes an experimental consistency condition. Crucially, this condition should be valid independent of the system details. When the system is in a regime in which Eq. (30) is violated according to the semiclassical prediction, one of these two experimental outcomes is possible: (i) The experimental data complies with Eq. (30). This implies that there are emergent collective quantum correlations not captured by the semiclassical model assuming independent atoms, which assist in the maintenance of Eq. (30) and gives rise to the elusive Heisenberg scaling. (ii) The experimental data violates Eq. (30). This would hint to a fundamental problem with the quantum description of light and matter, and possible with quantum mechanics itself, in particular if the predictions for the signal and noise would agree with the semiclassical model.

- *Model limitations.* Finally, we comment on the validity of the deployed models. Crucially, neither model will ideally describe the physical system in the whole parameter range. However, the limiting cases discussed here predict characteristic features, which can be identified in experiments.

Clearly, the semiclassical approach invalidates itself in the large atom number regime, apparent by the violation of the Cramer-Rao inequality, which can thus be deployed as a sanity check for theoretical investigations in spectroscopy. From Eq. (21), we learn that a violation is possible in the weak dissipation limit, i.e., in the deep quantum regime. A strong dissipation destroys any quantum correlations between the atoms and eventually restores the semiclassical validity.

The collective model assumes that the dissipative dynamics acts collectively on all atoms. This assumption is reasonable for the dissipators emitting photons in the propagation direction (i.e., the z direction) of the light beam, as it is not possible to identify the origin of a particular photon. However, for spontaneous photon emission in any other directions, the atom of origin can be—in principle—detected. This means that these processes will give rise to local dissipation, being detrimental to a collective atomic entanglement. Yet, the limitations of the semiclassical model reveal that the local dissipation may be insufficient to obstruct the Heisenberg scaling.

IV. OUTLOOK

This paper investigates intriguing quantum effects in the large-atom-number regime of optical magnetometers, and develops methods for their quantitative and qualitative investigation. A central result of this investigation is the breakdown of the semiclassical approximation in spectroscopy. The Cramer-Rao bound can thereby be regarded as a sanity check. The investigation of the collective model proposes to pinpoint the deficiency of the semiclassical approach to the neglected quantum correlations between the atoms. Interestingly, these quantum correlations can give rise to Heisenberg scaling of the quantum Fisher information.

The macroscopic character of the system imposes a theoretical challenge to describe the system in an accurate and microscopic fashion, as both local and collective dissipation processes must be modeled on an equal footing, requiring more advanced theoretical methods [87] and experimental investigations. The distinct predictions of the two limiting models (semiclassical and collective descriptions) offers guidelines for the interpretation of the results.

Our analysis has revealed that the collective model can exhibit Heisenberg scaling of the quantum Fisher information. The applied methods do not suggest how to take advantage of this fact, as the current investigation has considered time-integrated observables. A time-resolved analysis of the intensity fluctuations, e.g., using a Kalman filter similar to Ref. [62], can assess the possibility to take advantage of the Heisenberg scaling in magnetic field sensing.

Heisenberg scaling has been predicted in the previous literature, yet, induced by physical interactions. The present investigation suggest that also measurement-induced quantum correlations can induce Heisenberg scaling, even in a dissipative stationary state. Thus, the emergent Heisenberg scaling predicted here can be viewed as a new paradigm in quantum sensing, asking for future experimental and theoretical attention.

ACKNOWLEDGMENTS

G.E. acknowledges the support by the National Natural Science Foundation of China (Grant No. W2432004). X.W. acknowledges the National Natural Science Foundation of China (Grant No. 12404409) and the support of the SUSTech Presidential Postdoctoral Fellowship. J.Y.L. acknowledges the support from the National Natural Science Foundation of China (Grant Nos. 11774311). J.F.C acknowledges (NSFC) through Grants No. 92476102, No. 92265109 and the Guangdong Key Project under Grant No. 2022B1515020096.

Numerical data and corresponding source code are openly available at Ref. [88].

Appendix A: Fisher information

In this Appendix, we review basic properties of the quantum and classical Fisher information for self consistency.

1. Modified Cramer-Rao bound

Here, we derive the representation of the Fisher information in Eq. (6) for Hamiltonian parameter estimation using an argument from linear-response theory. For a more general derivation, we refer to Ref. [80]. Thereby, we assume that the Hamiltonian depends on the parameter to be measured X , i.e., $\hat{H} = \hat{H}_X$.

Applying the Heisenberg inequality to an arbitrary operator \hat{A} and the operator

$$\hat{\mathcal{F}} = \int_0^\tau \partial_X \hat{H}_X(t) dt, \quad (A1)$$

we obtain

$$\begin{aligned} \langle \Delta \hat{\mathcal{F}}^2 \rangle \langle \Delta \hat{A}^2 \rangle &\equiv \left\langle \left(\hat{\mathcal{F}} - \langle \hat{\mathcal{F}} \rangle \right)^2 \right\rangle \left\langle \left(\hat{A} - \langle \hat{A} \rangle \right)^2 \right\rangle \\ &\geq \frac{1}{4} \left| \left\langle [\hat{\mathcal{F}}, \hat{A}] \right\rangle \right|^2 \\ &= \frac{1}{4} \left| \int_0^\tau dt \left\langle [\partial_X \hat{H}_X(t), \hat{A}] \right\rangle \right|^2, \end{aligned} \quad (A2)$$

where the expectation value refers to the initial state of the joint light-matter state. Within linear-response theory, we can identify

$$\int_0^\tau dt \left\langle [\partial_X \hat{H}_X(t), \hat{A}] \right\rangle = \left\langle \frac{d\hat{A}}{dX} \right\rangle \quad (A3)$$

as the response of the observable \hat{A} for a small perturbation of the Hamiltonian in X . Convincing ourselves that

$$\mathcal{I}_X^{(Q)} = 4 \left\langle \left(\hat{\mathcal{F}} - \langle \hat{\mathcal{F}} \rangle \right)^2 \right\rangle, \quad (A4)$$

where $\mathcal{I}_X^{(Q)}$ is the quantum Fisher information defined in Eq. (5), we obtain the inequality

$$\mathcal{I}_X^{(Q)} \geq \frac{\left\langle \partial_X \hat{A} \right\rangle^2}{\langle \Delta \hat{A}^2 \rangle}, \quad (A5)$$

which is a modified version of the celebrated Cramer-Rao bound. As there is always an operator which fulfills the equality in Eq. (A2), we finally obtain the representation in Eq. (6). Noteworthy, Eq. (A5) is also valid for continuous measurements (such as in optical magnetometry),

as a continuous measurement in time can be mapped to instantaneous measurement in position space.

2. Quantum Fisher information

Here we provide alternative expressions for the quantum Fisher information in Eq. (5) which are easier to evaluate. The time-evolved wave function at time τ reads

$$|\Psi_X\rangle = e^{-i\hat{H}_X\tau}|\Psi(0)\rangle, \quad (\text{A6})$$

where $|\Psi(0)\rangle$ denotes the initial state. We now show that the Fisher information can be expressed as [81]

$$\mathcal{I}_X^{(Q)} = 4 \left[\langle \partial_X \Psi_X | \partial_X \Psi_X \rangle - |\langle \Psi_X | \partial_X \Psi_X \rangle|^2 \right]. \quad (\text{A7})$$

Without loss of generality, we consider the Fisher information at $X = 0$. To this end, we expand

$$\hat{H}_X = \hat{H}_0 + \hat{F}X + \mathcal{O}[X^2], \quad (\text{A8})$$

where $\hat{F} = \partial_X \hat{H}_{X=0}$. The time-evolution operator in Eq. (A6) can be expressed as

$$e^{-i\hat{H}_X t} = e^{-i\hat{H}_0 t} \hat{U}_X(t), \quad (\text{A9})$$

where $\hat{U}_X(t)$ is the time-evolution operator in the interaction picture defined by $\hat{H}_{X=0}$. Expanding in orders of X , it reads

$$\hat{U}_X(t) = 1 - iX \int_0^t dt \hat{F}(t) + \mathcal{O}(X^2), \quad (\text{A10})$$

where the time dependence of $\hat{F}(t)$ is determined by \hat{H}_0 . Using this expression to evaluate Eq. (A7), we directly find the integral form of the Fisher information in Eq. (5).

Alternatively, the Fisher information in Eq. (A7) can be expressed as

$$\begin{aligned} \mathcal{I}_X^{(Q)} &= -\partial_\delta^2 \log \text{tr} [\rho_\delta(\tau)]_{\delta=0}, \\ \rho_\delta(\tau) &= |\Psi_\delta\rangle \langle \Psi_{-\delta}|, \end{aligned} \quad (\text{A11})$$

which is a modified version of the ones in Refs. [57, 70]. This expression is suitable for the evaluation in open quantum systems, where the time-dependence of the density matrix ρ_δ can be obtained by integrating a generalized master equation

$$\begin{aligned} \frac{d}{dt} \rho_\delta &= \mathcal{L}_\delta \rho_\delta \\ &= -i [H_{M,\delta} \rho_\delta - \rho_\delta H_{M,-\delta}] + \mathcal{L}^D \rho_\delta, \end{aligned} \quad (\text{A12})$$

as can be seen by comparing Eqs. (A7) and Eq. (A6). Thereby, we assume that only the matter contribution of the Hamiltonian $H_{M,X}$ parametrically depends on X , while the terms giving rise to dissipation (described by

\mathcal{L}^D) are independent of X .

In the long-time limit, the quantum Fisher information can be efficiently evaluated using Eq. (A12) [57, 81]. Let us denote the eigenvalues and eigenvectors of the Liouvillian \mathcal{L}_δ by $\lambda_{a,\delta}$ and $\rho_{a,\delta}$. Labeling the eigenvectors such that $\lambda_{a=0,\delta}$ is $\lambda_{a=0,\delta=0} = 0$, we find in the long-time limit

$$\lim_{t \rightarrow \infty} \rho_\delta(t) = e^{\lambda_{0,\delta} t} \rho_{0,\delta}, \quad (\text{A13})$$

i.e., the generalized density matrix is dominated by the $a = 0$ eigenvalue. Using now Eqs. (A11), we find the asymptotic behavior of the quantum Fisher information

$$\mathcal{I}_X^{(Q)}(t) = -\partial_\delta^2 \lambda_{0,\delta}|_{\delta=0} t + (1), \quad (\text{A14})$$

which can be efficiently evaluated numerically.

Appendix B: Quantum-trajectory approach

To calculate the statistics of the photons measured by the detector, we employ a quantum-trajectory approach as in Ref. [65, 66], amended with methods from full-counting statistics similar as in Ref. [67], but here we generalize the approach to coherent driving fields.

1. Full-counting statistics

We are interested into the measurement statistics of a set of photonic occupation operators $\hat{n}_\xi = \hat{a}_\xi^\dagger \hat{a}_\xi$, which will be specified in Sec. B 2. The corresponding photon numbers are denoted by n_ξ . In terms of the photonic probabilities $p_{\mathbf{n}}$, where $\mathbf{n} = (n_1, \dots, n_{\xi_{\max}})$ is a vector of photon numbers, the moment- and cumulant generating functions are defined as

$$\begin{aligned} M_{\boldsymbol{\chi}} &\equiv \sum_{\mathbf{n}} p_{\mathbf{n}} e^{-i\boldsymbol{\chi} \cdot \mathbf{n}} = \text{tr} [e^{-i\boldsymbol{\chi} \cdot \hat{\mathbf{n}}} \rho_{\text{tot}}], \\ K_{\boldsymbol{\chi}} &\equiv \log M_{\boldsymbol{\chi}}, \end{aligned} \quad (\text{B1})$$

where ρ_{tot} denotes the density matrix of the full system, and $\text{tr}[\bullet]$ is the trace over all degrees of freedom. The parameters $\boldsymbol{\chi} = (\chi_1, \dots, \chi_{\xi_{\max}})$ are the so-called counting fields conjugated to the photon numbers.

The derivatives of the cumulant-generating function with respect to the counting fields, generate the cumulants of the probability distribution. For instance, the first- and second-order cumulants,

$$\begin{aligned} \kappa_1^{(\xi)} &\equiv \partial_\xi K_{\boldsymbol{\chi}=\mathbf{0}} = \langle \hat{n}_\xi(t) \rangle = \bar{n}_k, \\ \kappa_2^{(\xi)} &\equiv \partial_\xi^2 K_{\boldsymbol{\chi}=\mathbf{0}} = \langle \hat{n}_\xi^2 \rangle - \langle \hat{n}_k \rangle^2, \end{aligned} \quad (\text{B2})$$

are the mean and the variance of the photonic probability distribution. Likewise, mixed derivatives produce covariances of the probability distribution. Higher-order-cumulants provide information about the deviation of the

probability distribution from a Gaussian distribution.

2. Generalized master equation

In this Appendix, we derive an expression for the moment-generating function of the photonic field after interaction with the matter system located at a particular position \mathbf{r} which is on an equal footing with the quantum trajectory approach [66, 67]. For the semiclassical model, the matter system is a single atom. For the collective model, the matter system is described by a collective spin representing the whole ensemble of atoms, which are all assumed to be located at position \mathbf{r} .

In either case, the Hamiltonian Eq. (2) in an interaction picture defined by the unperturbed matter and photonic systems can be represented as

$$\hat{H}_\xi(t) = \sum_\xi \hat{H}_\xi(t) + \hat{H}_{\text{SE}}(t), \quad (\text{B3})$$

where

$$\hat{H}_\xi(t) = G_\xi(t) \left[\tilde{V}_\xi^{(-)}(t) \hat{a}_\xi^\dagger + \text{h.c.} \right], \quad (\text{B4})$$

describes the light-matter interaction between the matter system and the laser field. The photon operators $\hat{a}_\xi, \hat{a}_\xi^\dagger$ quantize the photonic field corresponding to the laser, where $\xi = (\eta, t_\xi)$ labels the polarization direction η as well as the time t_ξ at which the photonic operator \hat{a}_ξ interacts with matter system. Thereby, the photonic operators can be imagined to quantize a train of laser pulses propagating in the positive z direction, which couples to the matter operator $\tilde{V}_\xi^{(-)}$ during a time interval of infinitesimal length dt . The strength and time of the light-matter interaction is parameterized by $G_\xi(t) = g_\xi \delta(t - t_\xi) \propto dt^{-1/2}$. This light-matter interaction Hamiltonian can be strictly derived in terms of the windowed Fourier transformation [89]. The light-matter interaction not related to the laser field are absorbed into the system-environment Hamiltonian \hat{H}_{SE} , which describes spontaneous photon-emission or other environmental induced dissipation effects.

After interaction of the radiation field with the matter system, the moment-generating function defined in

Eq. (B1) is given by

$$M_{\mathbf{x}}(\tau) = \text{tr} \left[e^{-i\mathbf{x} \cdot \mathbf{n}} \tilde{U}(0, \tau) \rho_{\text{tot}}(0) \tilde{U}^\dagger(0, \tau) \right], \quad (\text{B5})$$

where $\tilde{U}(0, \tau)$ denotes the time-evolution operator corresponding to Eq. (B3), and the initial condition of the light-matter interaction is given by

$$\rho_{\text{tot}}(0) = \rho_M(0) \otimes \prod_\xi |\alpha_\xi\rangle \langle \alpha_\xi|. \quad (\text{B6})$$

Thereby, $\rho_M(0)$ is the matter density matrix, and $|\alpha_\xi\rangle$ denotes a photonic coherent state of the mode \hat{a}_ξ , i.e., $\hat{a}_\xi |\alpha_\xi\rangle = \alpha_\xi |\alpha_\xi\rangle$. To obtain a well-defined scaling when setting up the master equation, we assume that $|\alpha_\xi|^2 = \dot{\nu}_\xi dt$ with a real-valued photon flux $\dot{\nu}_\xi = d\nu_\xi/dt$ attributed to the mode \hat{a}_ξ , where dt denotes the time increment.

For small time-increments dt , the time-evolution operator \tilde{U} can be expanded as

$$\begin{aligned} \tilde{U}(t, t+dt) &= 1 - idt \sum_\xi \hat{H}_\xi(t) \\ &\quad - dt^2 \sum_{\xi_1, \xi_2} \hat{H}_{\xi_1}(t) \hat{H}_{\xi_2}(t) \\ &\quad + \mathcal{O} [G_\xi^3(t)]. \end{aligned} \quad (\text{B7})$$

As the light-matter coupling parameters $G_\xi(t)$ interact with the quantum system only in a particular instant of time, we can neglect higher expansion orders within the Markov assumption in the quantum trajectory approach.

Let us define now the generalized density matrix of the matter system at time t via the relation

$$\tilde{\rho}_{\mathbf{x}}(t) = \text{tr}_L \left[e^{-i\sum_{t' \leq t} \mathbf{x}_{t'} \cdot \mathbf{n}} \tilde{U}(0, t) \rho_{\text{tot}}(0) \tilde{U}^\dagger(0, t) \right], \quad (\text{B8})$$

where $\text{tr}_L [\bullet]$ denotes the trace over the photonic degrees of freedom. We have defined \mathbf{x}_t as the vector of counting fields whose corresponding photonic operators interact with the matter system at time t .

The next step is to express $\tilde{\rho}_{\mathbf{x}}(t+dt)$ in terms of $\tilde{\rho}_{\mathbf{x}}(t)$ and the time-evolution operator in Eq. (B7). Let us denote the set of photonic modes, which are going to interact with the matter system during the time interval $(t, t+dt)$ by Λ_t . Then we can evaluate

$$\begin{aligned} \tilde{\rho}_{\mathbf{x}}(t+dt) &\equiv \text{tr}_L \left[e^{-i\mathbf{x}_{t+dt} \cdot \mathbf{n}} U(t, t+dt) \tilde{\rho}_{\mathbf{x}}(t) \prod_{\xi \in \Lambda_t} |\alpha_\xi\rangle \langle \alpha_\xi| U^\dagger(t, t+dt) \right] \\ &= \tilde{\rho}_{\mathbf{x}} M_{\mathbf{x}, \Lambda_t}(0) \\ &\quad - idt \sum_{\xi \in \Lambda_t} \left[G_\xi(t) \left(\alpha_\xi^* \tilde{V}_\xi^{(-)}(t) e^{-i\chi_\xi} + \alpha_\xi \tilde{V}_\xi^{(+)}(t) \right) \tilde{\rho}_{\mathbf{x}} + i \tilde{\rho}_{\mathbf{x}} G_\xi(t) \left(\alpha_\xi^* \tilde{V}_\xi^{(-)}(t) + \alpha_\xi \tilde{V}_\xi^{(+)}(t) e^{-i\chi_\xi} \right) \right] M_{\mathbf{x}, \Lambda_t}(0) \end{aligned}$$

$$\begin{aligned}
& + dt^2 \sum_{\xi \in \Lambda_t} \left[e^{-i\chi_\xi} G_\xi^2(t) \tilde{V}_\xi^{(-)}(t) \tilde{\rho}_\chi \tilde{V}_\xi^{(+)}(t) - \frac{1}{2} G_\xi^2(t) \left\{ \tilde{V}_\xi^{(+)}(t) \tilde{V}_{m,\xi}^{(-)}(t), \tilde{\rho}_\chi \right\} \right] M_{\chi, \Lambda_t}(0)) \\
& + \mathcal{O}[G_\xi^3(t)],
\end{aligned} \tag{B9}$$

where we have utilized

$$\hat{a}_\xi e^{-i\chi_\xi \hat{n}_\xi} = e^{-i\chi_\xi \hat{n}_\xi} \hat{a}_\xi e^{-i\chi_\xi} \tag{B10}$$

and

$$\langle \alpha_\xi | e^{-i\chi_\xi \cdot \hat{n}_\xi} | \alpha_\xi \rangle = \exp \left[(e^{-i\chi_\xi} - 1) |\alpha_\xi|^2 \right], \tag{B11}$$

which is the moment-generating function of the Poisson distribution. These terms give rise to the initial moment-generating function

$$M_{\chi, \Lambda_t}(0) = \prod_{\xi \in \Lambda_t} \exp \left[(e^{-i\chi_\xi} - 1) \nu_\xi \right], \tag{B12}$$

of the modes $\xi \in \Lambda_t$, where we have introduced $\nu_\xi = |\alpha_\xi|^2$.

Using Eq. (B9), we can derive an expression for the final moment-generating function

$$M_{\chi|\nu}(\tau) = M_{dy, \chi|\nu}(\tau) M_{\chi|\nu}(0), \tag{B13}$$

where

$$M_{\chi|\nu}(0) = \prod_{\xi} \exp \left[(e^{-i\chi_\xi} - 1) \nu_\xi \right]. \tag{B14}$$

The term $M_{dy, \chi|\nu}(t_p)$ is denoted as the dynamical moment-generating function and is given by

$$M_{dy, \chi|\nu}(\tau) = \text{tr} [\rho_\chi(\tau)], \tag{B15}$$

where ρ_χ is the reduced density matrix. It can be obtained by the solution of the generalized master equation

$$\begin{aligned}
\frac{d}{dt} \rho_\chi & = -i \left[\hat{\mathcal{H}}_\chi(t) \rho_\chi - \rho_\chi \hat{\mathcal{H}}_\chi^\dagger(t) \right] \\
& + \mathcal{L}_\chi^D(t) \rho_\chi + \mathcal{L}^D \rho_\chi,
\end{aligned} \tag{B16}$$

where the non-Hermitian Hamiltonian is given by

$$\hat{\mathcal{H}}_\chi(t) = \sum_{\xi} G_\xi(t) \left(\alpha_\xi^* \tilde{V}_\xi^{(-)}(t) e^{-i\chi_\xi} + \alpha_\xi \tilde{V}_\xi^{(+)}(t) \right). \tag{B17}$$

Importantly, the non-Hermitian character of the generalized master equation encodes the counting statistics of the photons. The counting-field-dependent dissipation terms in Eq. (B16) are given by

$$\mathcal{L}_\chi^D(t) \rho = \sum_{\xi} dt G_\xi^2(t) D_{\chi_\xi} [\tilde{V}_\xi^{(-)}(t)] \rho,$$

where

$$D_\chi[\hat{O}] \rho = e^{-i\chi} \hat{O} \rho \hat{O}^\dagger + \frac{1}{2} \left\{ \hat{O}^\dagger \hat{O}, \rho \right\} \tag{B18}$$

is a counting-field-dependent dissipator. Using the moment-generating function in Eq. (B13), we can calculate the cumulants of the photonic probability distribution using Eq. (B2). To relate $G_\xi(t)$ to physical quantities, we introduce

$$\begin{aligned}
\Omega_\xi & = 2G_\xi(t)\alpha_\xi, \\
\gamma_{z,\xi} & = dt G_\xi^2(t)
\end{aligned} \tag{B19}$$

as the Rabi frequency and spontaneous emission rate in positive z direction. Reminding ourselves that $|\alpha_\xi|^2 = \dot{\nu}_\xi dt$ with photon flux $\dot{\nu}_\xi = d\nu_\xi/dt$, we find the relation

$$\gamma_{z,\xi} = \frac{|\Omega_\xi|^2}{4\dot{\nu}_\xi}, \tag{B20}$$

which must be fulfilled to guarantee microscopic consistency of the generalized master equation in Eq. (B16). In experiments, the Rabi frequency and the photon flux can be easily determined, from which we can then obtain a consistent $\gamma_{z,\xi}$.

In the semiclassical treatment of spectroscopy, the spontaneous emission rates $\gamma_{z,\xi}$ are extremely small, such that the number of spontaneously emitted photons in the z direction is negligibly small. However, these terms can contribute significantly to the photon emission in the collective model. Phenomenologically, we have added another dissipation term $\mathcal{L}^D \rho_\chi$, which accounts for spontaneous emission not along the z direction as described by \hat{H}_{SE} in Eq. (B3), or other optical pumping terms.

3. Time-integrated polarization measurements

In the previous derivation, we have assumed a generic time-resolved measurement, which has attributed to each time increment its own counting field χ_ξ with $\xi = (\eta, t_\xi)$, where $\eta \in \{\text{x}, \text{y}\}$ denotes the polarization direction. As explained in Eq. (7), we are interested into time-integrated measurements, which distinguish only between the polarization degrees. Inspection of the moment-generation in Eq. (B1) reveals, that this can be simply achieved by setting

$$\chi_\xi = \chi_\eta, \tag{B21}$$

that is, neglecting the time dependence of the counting-field label.

This simplifies the evaluation of the cumulants. As the Fisher information in Eq. (A11) has a similar structure as the cumulant-generating function of time-integrated photon numbers,

$$K_{\chi|\nu}(\tau) \equiv \log \text{tr} [\rho_{\chi}(\tau)] \log M_{\chi|\nu}(0), \quad (\text{B22})$$

i.e., the logarithm of the trace of a generalized density matrix, the cumulants of $K_{\chi|\nu}$ for long measurement times τ can be obtained in a similar fashion as in Eq. (A14) [90].

4. Integral expression of the cumulants

In Appendix B 2, we explained how to calculate the cumulants of the photonic probability distribution using the generalized master equation. Here, we show how the cumulants can be expressed in an integral form as given in the main text. For simplicity, we restrict the explanations to a single counting field χ .

To this end, we distribute the terms in the generalized master equation in Eq. (B16) in the following form

$$\frac{d}{dt} \rho_{\chi} = \mathcal{L}_0(t) \rho_{\chi} + \mathcal{L}_{1,\chi}(t) \rho_{\chi}, \quad (\text{B23})$$

where the Liouvillian \mathcal{L}_0 describes the dynamics of the density matrix for $\chi = 0$, and the counting-field-dependent terms are contained in $\mathcal{L}_{1,\chi}$.

A formal solution of Eq. (B23) is given by

$$\begin{aligned} \rho_{\chi}(t) &= \mathcal{T} \exp \left[\int_0^t dt_1 \tilde{\mathcal{L}}_{1,\chi}(t_1) \right] \rho(0) \\ &= \rho(0) + \int_0^t dt \tilde{\mathcal{L}}_{1,\chi}(t) \rho(0) \\ &+ \int_0^t dt_1 \int_0^{t_1} dt_2 \tilde{\mathcal{L}}_{1,\chi}(t_1) \tilde{\mathcal{L}}_{1,\chi}(t_2) \rho(0) \\ &+ \dots, \end{aligned} \quad (\text{B24})$$

where \mathcal{T} denotes the time-ordering operator and

$$\tilde{\mathcal{L}}_{\chi}(t) \equiv \mathcal{U}^{-1}(t) \mathcal{L}_{\chi}(t) \mathcal{U}(t) \quad (\text{B25})$$

is the counting-field-dependent Liouvillian transformed into an interaction picture defined by

$$\mathcal{U}(t) = \mathcal{T} e^{\int_0^t \mathcal{L}_0(t')}. \quad (\text{B26})$$

Thus the dynamical moment-generating function is given by

$$\begin{aligned} M_{\text{dy},\chi}(t) &= 1 + \int_0^t dt \left\langle \tilde{\mathcal{L}}_{1,\chi}(t) \right\rangle \\ &+ \int_0^t dt_1 \int_0^{t_1} dt_2 \left\langle \tilde{\mathcal{L}}_{1,\chi}(t_1) \tilde{\mathcal{L}}_{1,\chi}(t_2) \right\rangle \end{aligned}$$

$$+ \dots, \quad (\text{B27})$$

where the expectation values $\langle \bullet \rangle$ must be evaluated with respect to $\rho(0)$.

Using Eq. (B2) and Eq. (B27), we can now find integral expressions for the first two cumulants:

$$\kappa_1(\tau) = \int_0^{\tau} dt \left\langle \tilde{\mathcal{J}}^{(1)}(t) \right\rangle, \quad (\text{B28})$$

$$\begin{aligned} \kappa_2(\tau) &= \int_0^{\tau} dt \left\langle \tilde{\mathcal{J}}^{(2)}(t) \right\rangle \\ &+ \int_0^{\tau} dt_1 \int_0^{t_1} dt_2 \left\langle \Delta \tilde{\mathcal{J}}^{(1)}(t_1) \Delta \tilde{\mathcal{J}}^{(1)}(t_2) \right\rangle \end{aligned} \quad (\text{B29})$$

where we have introduced

$$\begin{aligned} \tilde{\mathcal{J}}^{(1)}(t) &= \partial_{\chi} \tilde{\mathcal{L}}_{1,\chi=0}(t) + \tilde{\mathcal{J}}^{(0)}(t), \\ \tilde{\mathcal{J}}^{(2)}(t) &= \partial_{\chi}^2 \tilde{\mathcal{L}}_{1,\chi=0}(t). \end{aligned} \quad (\text{B30})$$

Thereby, the operator $\tilde{\mathcal{J}}^{(0)}$ describes the photonic statistics before the light-matter interaction as given by $M_{\chi|\nu}(0)$ in Eq. (B13), and $\Delta \tilde{\mathcal{J}}^{(1)}(t) = \tilde{\mathcal{J}}^{(1)}(t_1) - \langle \tilde{\mathcal{J}}^{(1)}(t) \rangle$. While the integral representations in Eq. (B29) allows for a clear physical interpretation of the terms, the numerical evaluation via solving the generalized master equation in Eq. (B23) to construct the cumulant-generating function is numerically more efficient.

Appendix C: Semiclassical treatment

Because of the macroscopic number of quantum-emitters, it is not possible to treat the system in a fully microscopic fashion within the quantum trajectory framework. To obtain quantitative predictions, we develop here a hybrid semiclassical-quantum-trajectory approach based on successive light-atom interactions.

1. Semiclassical flow equations

In the semiclassical framework, we consider *stochastic* photonic mean fields $\nu_{\eta} = |\alpha_{\eta}|^2$, where α_{η} describes the coherent photonic state in Eq. (B6) with polarization direction $\eta \in \{\text{x}, \text{y}\}$. The following treatment focuses on the first- and second-order cumulants, which we investigate in this work.

The stochastic mean fields are described by the probability distribution $p_{\nu}(z)$ (where z refers here to a position within the atomic cloud). During the propagation of the photonic field through the quantum emitter ensemble, the probability distribution will be continuously updated according to the light-matter interaction. In the following, we derive and analyze flow equations for the low-order cumulants of $p_{\nu}(z)$. Crucially, we thus distinguish

between the photonic probability distribution $p_{\nu}(z)$ and the stochastic mean-field probability distribution $p_{\nu}(z)$.

We derive the flow equations in term of the averaged moment-generating function defined as

$$\overline{M}_{\chi}(z) = \int d\nu p_{\nu}(z) M_{\chi|\nu}(z), \quad (\text{C1})$$

where $M_{\chi|\nu}(z)$ is the moment-generating function for the photonic probability distribution in Eq. (B13) conditioned on a specific coherent mean-field value ν . We now determine the updated probability distribution $p_{\nu}(z + dz)$, such that we can represent the averaged moment-generating in Eq. (C1) in the form

$$\overline{M}_{\chi}(z) \equiv \int d\nu p_{\nu}(z + dz) e^{\nu \cdot (e^{i\chi} - 1)}. \quad (\text{C2})$$

where $e^{i\chi}$ refers to a component-wise evaluation of the counting-field vector χ . In other words, we aim to find a mean-field distribution, such that the resulting ensemble of coherent photonic states gives rise to the same photonic probability distribution as Eq. (C1).

As we are interested in describing the first two cumulants, we parameterize

$$p_{\nu}(z) = \frac{1}{2\pi \det \Sigma_z} \exp \left[-\frac{1}{2} (\nu - \bar{\nu}_z) \Sigma_z^{-2} (\nu - \bar{\nu}_z) \right] \quad (\text{C3})$$

where $\bar{\nu}_z$ denotes the vector of mean values of the stochastic mean field, and Σ_z^2 the corresponding covariance matrix. Moreover, when expanding the conditioned moment-generating function as

$$\begin{aligned} M_{\chi|\nu}(z) &= \exp \left(-i\kappa_{1,\nu} \cdot \chi - \frac{1}{2} \chi \kappa_{2,\nu} \chi + \mathcal{O}(\chi^3) \right) \\ &= \exp \left[-i\kappa_{1,\bar{\nu}_z} \cdot \chi - \frac{1}{2} \chi \kappa_{2,\bar{\nu}_z} \chi \right. \\ &\quad \left. - i \sum_{\eta=x,y} (\partial_{\bar{\nu}_\eta} \kappa_{1,\bar{\nu}_z} \cdot \chi) \tilde{\nu}_\eta + \mathcal{O}(\tilde{\nu}^2, \tilde{\nu} \chi^2, \chi^3) \right] \end{aligned} \quad (\text{C4})$$

where $\kappa_{1,\bar{\nu}_z}$ ($\kappa_{2,\bar{\nu}_z}$) denotes the vector (matrix) of first (second) order cumulants corresponding to the moment-generating function $M_{\chi|\nu}(z)$. In the second line, we have expanded the cumulants up to leading order in $\tilde{\nu} = \nu - \bar{\nu}_z$, as higher-order terms in the expansion do not influence the final flow equations. Because of the product form of the conditioned moment-generating function in Eq. (B13), we find

$$\begin{aligned} \kappa_{1,\nu} &= \nu + \kappa_{\text{dy},1,\nu}, \\ \kappa_{2,\nu} &= \text{diag } \nu + \kappa_{\text{dy},2,\nu}, \end{aligned} \quad (\text{C5})$$

where $\text{diag } \nu$ denote a diagonal matrix with diagonal el-

ements given by ν , and

$$\begin{aligned} [\kappa_{\text{dy},1,\nu}]_{\eta} &= \partial_{\chi_\eta} \log M_{\text{dy},\chi=0|\nu}(\tau), \\ [\kappa_{\text{dy},2,\nu}]_{\eta_1, \eta_2} &= \partial_{\chi_{\eta_1}} \partial_{\chi_{\eta_2}} \log M_{\text{dy},\chi=0|\nu}(\tau), \end{aligned} \quad (\text{C6})$$

will be denoted as the dynamical cumulants in the following.

Evaluating the Gaussian integral in Eq. (C1) using Eqs. (C3) and (C4), we obtain

$$\begin{aligned} \log \overline{M}_{\chi}(z) &= -i\kappa_{1,\bar{\nu}_z} \cdot \chi - \frac{1}{2} \chi \kappa_{2,\bar{\nu}_z} \chi \\ &\quad - \frac{1}{2} \sum_{\eta_1, \eta_2=x,y} (\partial_{\bar{\nu}_{\eta_1}} \kappa_{1,\bar{\nu}_z} \cdot \chi) [\Sigma_z^2]_{\eta_1 \eta_2} (\partial_{\bar{\nu}_{\eta_2}} \kappa_{1,\bar{\nu}_z} \cdot \chi) \\ &\quad + \mathcal{O}(\chi^3). \end{aligned} \quad (\text{C7})$$

Likewise, evaluating Eq. (C2) in the same order of χ , we obtain

$$\begin{aligned} \log \overline{M}_{\chi}(z) &= -i\bar{\nu}_{z+dz} \cdot \chi \\ &\quad - \frac{1}{2} \chi (\text{diag } \bar{\nu}_{z+dz} + \Sigma_{z+dz}^2) \chi + \mathcal{O}(\chi^3). \end{aligned} \quad (\text{C8})$$

Equating Eq. (C7) and (C8) and deriving with respect to the counting fields, we can construct flow equations for $\bar{\nu}_z$ and Σ_z . To this end, we introduce the position increment dz in such that $\rho_A \mathcal{A} dz = 1$ (atomic density ρ_A , laser cross section \mathcal{A}), i.e., the length dz of a unit volume $\mathcal{A} dz$ which contains on average one quantum emitter.

(i) The first derivative of Eqs. (C7) and (C8) with respect to the counting fields yields the flow equation for the mean of the stochastic mean field

$$\frac{d}{dz} \bar{\nu} = \mathbf{I}_{\bar{\nu}}, \quad (\text{C9})$$

where the coefficient is given by

$$[\mathbf{I}_{\bar{\nu}}]_{\eta} = \rho_A \mathcal{A} \partial_{\chi_\eta} \log M_{\text{dy},\chi|\bar{\nu}}(\tau). \quad (\text{C10})$$

Note that $\mathbf{I}_{\bar{\nu}}$ can depend on $\bar{\nu}$ in a nonlinear fashion.

(ii) The second derivative gives an equation for the covariance matrix of the stochastic mean field, and reads

$$\frac{d}{dz} \Sigma^2 = \mathbf{D}_{\bar{\nu}} + \mathbf{C}_{\bar{\nu}} \Sigma^2 + \Sigma^2 \mathbf{C}_{\bar{\nu}}, \quad (\text{C11})$$

where

$$[\mathbf{D}_{\bar{\nu}}]_{\eta_1, \eta_2} = \rho_A \mathcal{A} \partial_{\chi_{\eta_1}} \partial_{\chi_{\eta_2}} \log M_{\text{dy},\chi|\bar{\nu}}(\tau) - \text{diag}(\mathbf{I}_{\bar{\nu}}), \quad (\text{C12})$$

$$[\mathbf{C}_{\bar{\nu}}]_{\eta_1, \eta_2} = \rho_A \mathcal{A} \partial_{\bar{\nu}_{\eta_1}} \partial_{\zeta_{\eta_2}} \log M_{\text{dy},\chi|\bar{\nu}}(\tau). \quad (\text{C13})$$

will be denoted as the diffusion matrix and the phase-space matrix in the following. Note that we have neglected terms proportional to $\partial_{\bar{\nu}_{\eta_1}} \kappa_{1,\bar{\nu}_z} \partial_{\bar{\nu}_{\eta_2}} \kappa_{1,\bar{\nu}_z} \propto 1/(\bar{\nu}_{\eta_1} \bar{\nu}_{\eta_2})$ as they are suppressed for large mean fields

$$\bar{\nu}_{\eta_1}, \bar{\nu}_{\eta_2} \gg 1.$$

After integration of the flow equations, to obtain the statistics of the photon-number from the statistics of the stochastic mean field, we evaluate

$$\begin{aligned} \bar{\mathbf{n}}_z &= \bar{\nu}_z, \\ \Sigma_{\text{tot},z}^2 &= \Sigma_z^2 + \text{diag} \bar{\nu}_z, \end{aligned} \quad (\text{C14})$$

according to the moment-generating function of the photonic distribution in Eq. (C8). While the mean-photon number equals the mean of the stochastic mean field, the photon covariance matrix is a sum of the covariance matrix of the stochastic mean field and the photon-shot noise represented by $\bar{\nu}_z$. Noteworthy, the flow equations for the mean in Eq. (C9) and the variance in Eq. (C11) are formally equivalent to the one in the recently developed Photon-resolved Floquet theory, which is an ab-initio semiclassical approach to determine the photon number statistics [10], yet, which does not distinguishing between photon number and stochastic mean field. As Eq. (C9) is equivalent to the Maxwell-Bloch equation (which can be shown along the same lines as in [10]), the covariance flow equation (C11) can be considered as an generalization of this celebrated framework.

2. Statistics of polarization measurements

The measurement statistics of the polarization rotation in a magnetometer can be described using two photonic modes representing the two polarization directions of the linearly polarized light [i.e., the x and y directions in Fig. 1(a)]. We denote the photon-number operators by \hat{n}_x and \hat{n}_y . The related stochastic mean fields are ν_x and ν_y . In this Appendix, we provide practical guidelines how to evaluate the flow equations in Eqs. (C9) and (C11). Since the quantum trajectory approach developed in this work is closely related to the semiclassical approach of the Photon-resolve Floquet theory, we refer to Ref. [10] for more detailed explanations, and explain here merely the key steps.

It is convenient to describe the mean photon numbers in the form

$$\begin{pmatrix} \bar{n}_x \\ \bar{n}_y \end{pmatrix} = \bar{n}_+ \begin{pmatrix} \cos^2(\frac{\pi}{4} + \bar{\theta}) \\ \sin^2(\frac{\pi}{4} + \bar{\theta}) \end{pmatrix}, \quad (\text{C15})$$

where $\bar{n}_+ = \bar{n}_x + \bar{n}_y$ is the mean total photon number, and $\bar{\theta}$ is the mean rotation angle of the polarized light. These two quantities can be obtained by integration of the flow equations in a measurement basis rotated by $\bar{\theta}$: Denoting the corresponding photon number operators by $\bar{n}_{\text{rot},x}$ and $\bar{n}_{\text{rot},y}$, the rotated measurement basis fulfills $\bar{n}_{\text{rot},x} = \bar{n}_{\text{rot},y}$ for all z . In this basis, we obtain

$$\frac{d\bar{\theta}}{dz} = \frac{\partial_z \bar{n}_{\text{rot},x} - \partial_z \bar{n}_{\text{rot},y}}{2\bar{n}_+},$$

$$\frac{d\bar{n}_+}{dz} = \partial_z \bar{n}_{\text{rot},x} + \partial_z \bar{n}_{\text{rot},y}, \quad (\text{C16})$$

where

$$\partial_z \bar{n}_{\text{rot},\eta} = [\mathbf{I}_{\bar{\nu}_{\text{rot}}}]_\eta, \quad (\text{C17})$$

and $\mathbf{I}_{\bar{\nu}_{\text{rot}}}$ is the coefficient in Eq. (C10), but evaluated in the rotated measurement basis.

Now, we assume that

$$\check{I}_\eta = \frac{[\mathbf{I}_{\bar{\nu}_{\text{rot}}}]_\eta}{\bar{n}_+ \rho_A \mathcal{A}} = \text{const.}, \quad (\text{C18})$$

which is justified for off-resonant probe fields as in optical magnetometers. This physically means that \check{I}_α does not depend on the intensity of the probe field. In doing so, the flow equations become

$$\begin{aligned} \frac{d\bar{\theta}}{dz} &= \frac{\rho_A \mathcal{A}}{2} (\check{I}_x - \check{I}_y), \\ \frac{d\bar{n}_+}{dz} &= \rho_A \mathcal{A} (\check{I}_x + \check{I}_y) \bar{n}_+, \end{aligned} \quad (\text{C19})$$

whose analytical integration yields

$$\begin{aligned} \bar{\theta}(z) &= \frac{1}{2} \rho_A \mathcal{A} z (\check{I}_x - \check{I}_y), \\ \bar{n}_+(z) &= \bar{n}_+(0) e^{(\check{I}_x + \check{I}_y) \rho_A \mathcal{A} z}, \end{aligned} \quad (\text{C20})$$

where $\bar{n}_+(0)$ denotes the total photon number before the light-matter interaction.

We are interested into the statistics of the photon-number difference

$$\begin{aligned} \hat{n}_{\text{rot},-} &= \hat{n}_{\text{rot},x} - \hat{n}_{\text{rot},y} \\ &= \mathbf{v}_- \cdot \begin{pmatrix} \hat{n}_{\text{rot},x} \\ \hat{n}_{\text{rot},y} \end{pmatrix}, \end{aligned} \quad (\text{C21})$$

with $\mathbf{v}_- = (1, -1)$, from which we want to infer the unknown physical quantity X . Deriving the mean value of \hat{n}_- with respect to X yields

$$\begin{aligned} \frac{d\bar{n}_{\text{rot},-}}{dX} &= \bar{n}_{\text{rot},+} \frac{d\bar{\theta}}{dX} + \frac{d\bar{n}_{\text{rot},+}}{dX} \\ &= \rho_A \mathcal{A} z \frac{e^{(\check{I}_x + \check{I}_y) \rho_A \mathcal{A} z}}{2} \frac{d}{dX} (\check{I}_x - \check{I}_y) \\ &\quad + (\rho_A \mathcal{A} z)^2 \frac{e^{(\check{I}_x + \check{I}_y) \rho_A \mathcal{A} z}}{2} (\check{I}_x - \check{I}_y) \frac{d}{dX} (\check{I}_x + \check{I}_y). \end{aligned} \quad (\text{C22})$$

Note that we refer here to the derivative in a fixed rotated measurement basis specified by $\bar{\theta}$, as otherwise the derivative would exactly vanish because of the defining property $\bar{n}_{\text{rot},x} = \bar{n}_{\text{rot},y}$. The last term in Eq. (C22) describes photon absorption, and is vanishingly small for off-resonant measurements in an optical magnetometer. We note that Eq. (C22) is equivalent to Eq. (15) when

using the integral form of the coefficients and the fact that $N = \rho_A \mathcal{A} z$.

To estimate the signal-to-noise ratio $\mathcal{S}_X^{(n_{\text{rot}}, -)}$, we must evaluate the noise of \hat{n}_- . Using the close relation to the semiclassical treatment in Ref. [10], the noise can be evaluated using the following flow equation for the covariance matrix in the rotated measurement frame

$$\begin{aligned} \frac{d}{dz} \Sigma_{\text{rot}}^2 &= \mathbf{D}_{\bar{\nu}_{\text{rot}}} + \tilde{\mathbf{C}}_{\bar{\nu}_{\text{rot}}} \Sigma_{\text{rot}}^2 + \Sigma_{\text{rot}}^2 \tilde{\mathbf{C}}_{\bar{\nu}_{\text{rot}}}, \\ \tilde{\mathbf{C}}_{\bar{\nu}_{\text{rot}}} &= \mathbf{C}_{\bar{\nu}_{\text{rot}}} - \frac{d\bar{\theta}}{dz} \hat{\mathbf{\Xi}}, \end{aligned} \quad (\text{C23})$$

where $\hat{\mathbf{\Xi}} = \hat{\sigma}_z + i\sigma_y$. To proceed, we make the following assumption for the phase-space matrix and the diffusion matrix

$$\tilde{\mathbf{C}}_{\bar{\nu}_{\text{rot}}} = \rho_A \mathcal{A} \left(\check{I}_x + \check{I}_y \right) \mathbb{1}, \quad (\text{C24})$$

$$\check{D} = \frac{1}{\bar{n}_+^2} \frac{1}{\rho_A \mathcal{A}} \mathbf{v}_-^T \mathbf{D}_{\bar{\nu}_{\text{rot}}} \mathbf{v}_- = \text{const.}, \quad (\text{C25})$$

which is fulfilled for an off-resonant probe field (see also Sec. D 3).

The variance of \hat{n}_- is related to the covariance matrix in Eq. (C23) via

$$\Sigma_-^2 = \mathbf{v}_-^T \Sigma_{\text{rot}}^2 \mathbf{v}_-. \quad (\text{C26})$$

For the assumptions in Eq. (C25), the variance thus fulfills the following differential equation

$$\frac{d}{dz} \Sigma_-^2 = \rho_A \mathcal{A} \check{D} \bar{n}_+^2 + 2\rho_A \mathcal{A} \tilde{\mathbf{C}} \Sigma_-^2, \quad (\text{C27})$$

where $\bar{n}_+(z)$ is given in Eq. (C20) and $\tilde{\mathbf{C}} = \check{I}_x + \check{I}_y$. Analytical integration of Eq. (C27) yields

$$\Sigma_-(z) = \rho_A \mathcal{A} z \check{D} \bar{n}_+^2(0). \quad (\text{C28})$$

We recall that this represents the fluctuations of the stochastic mean field. To obtain the photon-number noise, we have to add the photon shot noise, such that we obtain

$$\Sigma_{\text{tot},-}(z) = \bar{n}_+(z) + \rho_A \mathcal{A} z \check{D} \bar{n}_+^2(0), \quad (\text{C29})$$

which is equivalent to Eq. (16).

Appendix D: Semiclassical model

Here, we describe the analysis of the optical magnetometer within the semiclassical model, i.e., for independent atoms. Starting from the four-level system in Eq. (2), we derive an effective two-level model, for which we can analytically obtain the measurement statistics of time-integrated photon numbers during the measurement interval $t \in [0, \tau]$.

1. Generalized master equation

Following the procedure in Appendix B 2, we construct the generalized master equation in Eq. (B16). In doing so, the semiclassical Hamiltonian corresponding to the microscopic Hamiltonian in Eq. (2) is given by

$$\begin{aligned} \hat{\mathcal{H}}_{m,\chi}(t) &= \hat{H}_{\text{M},m} \\ &+ \sum_{a=\pm} \frac{\Omega_{a,0}}{2} |e_{-a}\rangle \langle g_a| e^{-i\omega_p t} \\ &+ \sum_{a=\pm} \frac{\Omega_{a,\chi}^*}{2} |g_a\rangle \langle e_{-a}| e^{i\omega_p t}, \end{aligned} \quad (\text{D1})$$

where

$$\Omega_{a,\chi} = \Omega_x e^{i\chi_y} + ia\Omega_y e^{i\chi_y} \quad (\text{D2})$$

with $\Omega_\eta = 2G_\nu\alpha_\eta$ denoting the Rabi frequencies. Moreover, we assume a real-valued photonic amplitude $\alpha_\eta = \sqrt{\nu_\eta dt/\tau}$, where ν_η is the time-integrated stochastic mean field. For this choice, the coherent photonic field is indeed linearly polarized. The counting fields χ_x, χ_y are responsible for tracking the time-integrated measurement statistics of the photon number in the x and y polarization directions.

The counting-field-dependent dissipative Liouvillian is given by

$$\mathcal{L}_\chi^D \rho_\chi = \gamma_z \sum_{a=\pm 1} D_\chi [|g_a\rangle \langle e_{-a}|] \rho, \quad (\text{D3})$$

where $\gamma_z = \Omega_\eta^2 / 4\dot{\bar{\nu}}_\eta$ according to Eq. (B20). It connects states with different z-projection quantum numbers a . The generalized dissipator is defined in Eq. (B18).

The remaining dissipation terms are given by

$$\begin{aligned} \mathcal{L}^D \rho &= 2\gamma_D \sum_{a=\pm} D [|g_a\rangle \langle e_{-a}|] \rho \\ &+ \gamma_D \sum_{a=\pm 1} D [|g_a\rangle \langle e_a|] \rho \\ &+ \gamma_P D [(|g_1\rangle + |g_{-1}\rangle) (\langle g_1| - \langle g_{-1}|)] \rho, \end{aligned} \quad (\text{D4})$$

where γ_D is the spontaneous decay rate in a particular spatial direction (x, y, or z). Moreover, we have phenomenologically added a pumping term $\propto \gamma_P$, which polarizes the atoms in the positive x direction.

An optical magnetometer infers the strength of an external magnetic field by measuring the polarization rotation of linearly-polarized light as explained in Appendix C 2. To evaluate the signal in Eq. (C22) and the noise in Eq. (C29), we need the coefficients \check{I}_η and \check{D} . The dynamical moment-generating function is given by

$$\begin{aligned} \log M_{\text{dy},\chi|\nu}(\tau) &= \ln \text{tr} [\rho_\chi(\tau)] \\ &= \lambda_{0,\chi} \tau + \mathcal{O}(\tau^0), \end{aligned} \quad (\text{D5})$$

where ρ_{χ} is the reduced density matrix in Eq. (B16). In the second line, we have used the asymptotic behavior of the dynamical moment-generating function, where $\lambda_{0,\chi}$ is the dominating eigenvalue of the Liouvillian in Eq. (B16). Using Eq. (C10) and (C12), we can evaluate the desired coefficients \check{I}_{η} in Eq. (C18) and \check{D} in Eq. (C25). In the numerical calculations, we also verified that Eq. (C24) is fulfilled. In doing so, we have calculated the curves in Figs. 1 and Fig. 2 for the semiclassical four-level system.

Of note, as we are interested into $\check{I}_{\pm} = \check{I}_x \pm \check{I}_y$, we can replace $\chi_x = \chi_+ + \chi_-$ and $\chi_y = \chi_+ - \chi_-$ in the Liouvillian Eq. (B16), and derive the generating function with respect to χ_{\pm} to obtain \check{I}_{\pm} . This can be easily shown via the chain rule of derivation. Likewise, \check{D} is given by the second derivative with respect to χ_- .

2. Effective two-level system

To enable an analytical investigation, we derive here an effective two-level system, which inherits the essential physical properties of the four-level system in Eq. (D1). To this end, we first construct the equations of motions of the density matrix elements

$$\begin{aligned} \frac{d}{dt} \rho_{a,b}^{gg} &= -i h_{L,a,-a} \rho_{-a,b}^{gg} + i h_{R,b,-b}^* \rho_{a,-b}^{gg} \\ &\quad - i \frac{\Omega_{a,\chi}^*}{2} \rho_{-a,b}^{eg} + i \frac{\Omega_{b,-\chi}}{2} \rho_{a,-b}^{ge} \\ &\quad + 2\gamma_D \rho_{-a,-a}^{ee} \delta_{a,b} + \gamma_D \rho_{a,a}^{ee} \delta_{a,b} \\ &\quad + \gamma_P (\dots) + \gamma_z (\dots), \\ \frac{d}{dt} \rho_{a,b}^{eg} &= -i \epsilon_{\Delta} \rho_{a,b}^{eg} + i h_{R,b,-b}^* \rho_{a,-b}^{eg} \\ &\quad - i \frac{\Omega_{-a,0}}{2} \rho_{-a,b}^{gg} + i \frac{\Omega_{b,-\chi}}{2} \rho_{a,-b}^{ee} \\ &\quad - \frac{3\gamma_D}{2} \rho_{a,a}^{eg} \delta_{a,b} \\ &\quad + \gamma_P (\dots) + \gamma_z (\dots), \\ \frac{d}{dt} \rho_{a,b}^{ee} &= -i \frac{\Omega_{-a,0}}{2} \rho_{-a,b}^{ge} + i \frac{\Omega_{b,-\chi}}{2} \rho_{a,-b}^{eg} \\ &\quad - 3\gamma_D \rho_{a,a}^{ee} \delta_{a,b}, \end{aligned} \quad (D6)$$

where $h_{L,a,b}$ and $h_{R,a,b}$ are the matrix elements of Hamiltonian (D1) in the ground-state manifold. We have not explicitly specified the terms $\propto \gamma_P$ and $\propto \gamma_z$ for brevity. The adiabatic approximation assumes that $d\rho_{a,b}^{eg}/dt = 0$, such that

$$\rho_{a,b}^{eg} = \left(\rho_{a,b}^{ge} \right)^* \approx \frac{1}{2} \frac{-i\Omega_{-a,0}\rho_{-a,b}^{gg}}{i\epsilon_{\Delta} + \frac{\Gamma}{2}} + \mathcal{O} \left(\frac{\gamma_P \Omega}{\epsilon_{\Delta}^2}, \frac{\Omega^2}{\epsilon_{\Delta}^2} \right) \quad (D7)$$

for large detunings ϵ_{Δ} , where $\Gamma = 3\gamma_D + \gamma_z$ is the total relaxation rate. In the main text, we have expressed this in terms of $\gamma = 3\gamma_D$, which is the joint spontaneous decay rate in all three spatial directions. In the same spirit,

we also approximate the occupation of the excited-state manifold as

$$\rho_{a,a}^{ee} \approx \frac{1}{2} \frac{|\Omega_{-a,0}|^2}{\epsilon_{\Delta}^2 + \frac{\Gamma^2}{4}} \rho_{-a,-a}^{gg}. \quad (D8)$$

Inserting these expressions into the equations of motions of the ground states, we obtain the effective generalized master equation in the ground-state manifold

$$\begin{aligned} \frac{d}{dt} \rho_{\chi} &= -i \left[\hat{\mathcal{H}}_L \rho_{\chi} - \rho_{\chi} \hat{\mathcal{H}}_R \right] \\ &\quad + \gamma_P D \left[\frac{1}{2} (\hat{\sigma}_z + i\hat{\sigma}_y) \right] \rho_{\chi} \\ &\quad + \frac{\gamma}{\epsilon_{\Delta}^2 + \frac{\Gamma^2}{4}} \sum_a \Omega_{a,0}^* \Omega_{a,0} D [\hat{\pi}_a] \rho_{\chi} \\ &\quad + \frac{\Gamma}{\epsilon_{\Delta}^2 + \frac{\Gamma^2}{4}} \sum_a \Omega_{a,0} (\Omega_{a,\chi}^* - \Omega_{a,0}^*) \hat{\pi}_a \rho_{\chi} \\ &\quad + \frac{\Gamma}{\epsilon_{\Delta}^2 + \frac{\Gamma^2}{4}} \sum_a \Omega_{a,0}^* (\Omega_{a,\chi} - \Omega_{a,0}) \rho_{\chi} \hat{\pi}_a \\ &\quad + \frac{\gamma_z}{\epsilon_{\Delta}^2 + \frac{\Gamma^2}{4}} \sum_{\eta=x,y} \sum_{a=\pm 1} \Omega_{a,0}^* \Omega_{a,0} D_{\chi_{\eta}} [\hat{\pi}_{a,a}] \end{aligned} \quad (D9)$$

where

$$\begin{aligned} \hat{\mathcal{H}}_L &= -\frac{1}{2} \mathbf{h}_L \cdot \hat{\boldsymbol{\sigma}}, \\ \hat{\mathcal{H}}_R &= -\frac{1}{2} \mathbf{h}_R \cdot \hat{\boldsymbol{\sigma}}. \end{aligned} \quad (D10)$$

Thereby, $\hat{\boldsymbol{\sigma}} = (\sigma_x, \sigma_y, \sigma_z)$ is a vector of Pauli matrices, and the entries of the vectors \mathbf{h}_L and \mathbf{h}_R are given by

$$\begin{aligned} h_{L,x} &= h_{R,x} = \mu B_x, \\ h_{L,y} &= h_{R,y} = \mu B_y, \\ h_{L,z} &= \mu (B_z + \delta) + \mathcal{C}_{\chi} - \mathcal{C}_{-\chi}^*, \\ h_{R,z} &= \mu (B_z - \delta) - \mathcal{C}_{\chi} + \mathcal{C}_{-\chi}^*, \end{aligned} \quad (D11)$$

where

$$\mathcal{C}_{\chi} = \frac{\epsilon_{\Delta}}{(\epsilon_{\Delta}^2 + \frac{\Gamma^2}{4})} (\Omega_x + i\Omega_y) (\Omega_x e^{-i\chi_y} - i\Omega_y e^{-i\chi_y}) \quad (D12)$$

tracks the influence of the excited states. Note that we have assumed real valued Ω_x, Ω_y (corresponding to linearly polarized light) to reach this expression. We have included also the parameter δ as an auxiliary parameter to calculate the quantum Fisher information according to Eq. (A12). It is easy to see that Eq. (D9) reduces to Eq. (10) for $\chi = \mathbf{0}$ and $\delta = 0$.

3. Analytical calculations

To efficiently calculate the first two cumulants in the long-time limit according to Eq. (D5), we take advantage

of an expansion method for the characteristic polynomial of the Liouvillian in Eq. (B16) [84]. The characteristic polynomial can be expanded as

$$\mathcal{P}(z) = \sum a_j z^j. \quad (\text{D13})$$

We denote the derivatives of the expansion coefficients by

$$\begin{aligned} a_j^{(\eta)} &= \left. \frac{d}{d\chi_\eta} a_j \right|_{\chi=0}, \\ a_j^{(\eta\zeta)} &= \left. \frac{d}{d\chi_\eta} \frac{d}{d\chi_\zeta} a_j \right|_{\chi=0}, \end{aligned} \quad (\text{D14})$$

where $\eta, \zeta \in \{x, y, +, -\}$ depending on the observable of interest. The first derivative is given by

$$\frac{\partial}{\partial \chi_\alpha} \lambda_{0;\chi=0} = \frac{a_0^{(\eta)}}{a_1}, \quad (\text{D15})$$

while the second derivatives can be evaluated via

$$\frac{\partial^2 \lambda_{0;\chi=0}}{\partial \chi_\alpha \partial \chi_\beta} = \frac{a_0^{(\alpha\beta)}}{a_1} - \frac{a_0^{(\alpha)} a_1^{(\beta)} + a_0^{(\beta)} a_1^{(\alpha)}}{a_1^2} + \frac{2a_2 a_0^{(\alpha)} a_0^{(\beta)}}{a_1^3}. \quad (\text{D16})$$

For $\gamma_z = \gamma = 0$, it is possible to find a compact expression for the expansion coefficients of the characteristic polynomial:

$$\begin{aligned} a_4 &= 1, \\ a_3 &= 2\gamma_P, \\ a_2 &= \frac{1}{2} (h_L^2 + h_R^2) + h_x^2 + \frac{5}{4} \gamma_P^2, \\ a_1 &= \frac{\gamma_P}{2} (h_L - h_R)^2 + \frac{\gamma_P}{2} h_L h_R + \gamma_P h_x^2 + \frac{\gamma_P^3}{4}, \\ a_0 &= \frac{1}{16} (h_L^2 - h_R^2)^2 + \frac{\gamma_P^2}{8} (h_L - h_R)^2 + i h_x \gamma_P (h_L^2 - h_R^2), \end{aligned} \quad (\text{D17})$$

for finite χ and δ .

Consequently, the relevant derivatives with respect to $\chi = 0$ are given by

$$\begin{aligned} a_0 &= 0, \\ a_1 &= \frac{\gamma_P}{2} h_z^2 + \gamma_P h_x^2 + \frac{\gamma_P^3}{4}, \\ a_2 &= h_z^2 + h_x^2 + \frac{5}{4} \gamma_P^2, \\ a_0^{(\alpha)} &= i 2 \gamma_P h_x h_z \operatorname{Re} \mathcal{C}_0^{(\eta)}, \\ a_1^{(\alpha)} &= 0, \\ a_2^{(\alpha)} &= 0, \\ a_0^{(-)} &= (32 h_z^2 + 4 \gamma_P^2) [2 \operatorname{Re} \mathcal{C}_0^{(-)}]^2. \end{aligned} \quad (\text{D18})$$

Putting everything together, we find

$$\begin{aligned} \check{I}_\alpha &= -i \frac{\tau}{\bar{n}_+} \frac{d}{d\chi_\alpha} \lambda_{0;\chi=0} \\ &= \frac{\tau}{\bar{n}_+} \frac{8 h_x h_z}{2 h_z^2 + 4 h_x^2 + \gamma_P^2} \operatorname{Re} \mathcal{C}_0^{(\eta)}, \end{aligned} \quad (\text{D19})$$

where $\mathcal{C}_0^{(\eta)}$ refers to the derivative of \mathcal{C}_χ with respect to χ_η , which can be utilized to obtain the signal in Eq. (19). The diffusion coefficient for the photon-number difference becomes

$$\begin{aligned} \check{D} &= -\frac{\tau}{\bar{n}_+^2} \frac{d^2}{d^2 \chi_-} \lambda_{0;\chi=0} \\ &= \frac{\tau}{\bar{n}_+^2} \frac{8 h_z^2 + 4 \gamma_P^2}{2 \gamma_P h_z^2 + 4 \gamma_P h_x^2 + \gamma_P^3} [\operatorname{Re} \mathcal{C}_0^{(-)}]^2 \\ &\quad - 2 \frac{\tau}{\bar{n}_+^2} \frac{(h_z^2 + h_x^2 + \frac{5}{4} \gamma_P^2) (2 \gamma_P h_x h_z)^2}{(2 \gamma_P h_z^2 + 4 \gamma_P h_x^2 + \gamma_P^3)^3} [\operatorname{Re} \mathcal{C}_0^{(-)}]^2. \end{aligned} \quad (\text{D20})$$

Note that $\mathcal{C}_0 \propto \Omega^2 \propto \bar{n}_+$ such that \check{I}_α and \check{D} are indeed constants according to Eqs. (C18) and (C25). The phase-space matrix takes the form

$$\mathcal{C}_{\bar{n}_{\text{rot}}} = \rho_A \mathcal{A} \left(\check{I}_x - \check{I}_y \right) \begin{pmatrix} 1 & 1 \\ -1 & -1 \end{pmatrix}, \quad (\text{D21})$$

showing that the condition Eq. (C24) is fulfilled. Using now Eq. (C29), we obtain the measurement noise in Eq. (20).

In the same fashion, we can calculate the quantum Fisher information for a single atom by deriving the dominating eigenvalue two times with respect to δ , yielding

$$\begin{aligned} \mathcal{I}_{B_z}^{(Q)} &= -\tau \frac{d^2}{d^2 \delta} \lambda_{0;\delta=0} \\ &= \tau \frac{8 h_z^2 + 4 \gamma_P^2}{2 \gamma_P h_z^2 + 4 \gamma_P h_x^2 + \gamma_P^3} \mu^2 \\ &\quad - 2 \tau \frac{(h_z^2 + h_x^2 + \frac{5}{4} \gamma_P^2) (2 \gamma_P h_x h_z)^2}{(2 \gamma_P h_z^2 + 4 \gamma_P h_x^2 + \gamma_P^3)^3} \mu^2, \end{aligned} \quad (\text{D22})$$

which is remarkably similar to the noise in Eq. (D20).

Appendix E: Collective approach

Here, we analyze the situation when the atoms cannot be regarded as distinguishable quantum emitters. Then the ensemble of four-level atoms in Eq. (2) can be conveniently described by the collective operators

$$\hat{S}_{a,b} = \sum_m |g_{m,a}\rangle \langle g_{m,b}|,$$

$$\begin{aligned}\hat{J}_{a,b}^+ &= \sum_m |e_{m,a}\rangle \langle g_{m,b}|, \\ \hat{J}_{a,b}^- &= \hat{J}_{a,b}^{+\dagger},\end{aligned}\quad (\text{E1})$$

with $a, b \in \{1, -1\}$. The collective spin operators are defined by

$$\begin{aligned}\hat{S}_x &= \frac{1}{2} (\hat{S}_{1,-1} + \hat{S}_{-1,1}), \\ \hat{S}_y &\equiv \frac{1}{2i} (\hat{S}_{1,-1} - \hat{S}_{-1,1}), \\ \hat{S}_z &\equiv \frac{1}{2} (\hat{S}_{1,1} - \hat{S}_{-1,-1}),\end{aligned}\quad (\text{E2})$$

which abide to the common angular-momentum algebra. Denoting $\hat{N} = \hat{S}_{1,1} + \hat{S}_{-1,-1}$ as the number of atoms in the ground-state manifold, we also introduce

$$\hat{P}_a = \frac{1}{2} \hat{N} + a \hat{S}_z \quad (\text{E3})$$

as an operator counting the number of atoms in state $|g_{m,a}\rangle$.

1. Master equation

Using the formalism in Appendix B 2, we can establish a generalized quantum-master equation, which reads

$$\begin{aligned}\frac{d}{dt} \rho_{\chi} &= -i [\hat{\mathcal{H}}_L(t) \rho_{\chi} - \rho_{\chi} \hat{\mathcal{H}}_R(t)] \\ &+ \gamma_z \sum_{a=\pm} \sum_{\eta=\pm, y} D_{\chi\eta} [\hat{J}_{a,-a}^-] \rho_{\chi} \\ &+ 2\gamma_D \sum_{a=\pm} D[\hat{J}_{a,-a}^-] \rho_{\chi} \\ &+ \gamma_D \sum_{a=\pm} D[\hat{J}_{a,a}^-] \rho_{\chi}.\end{aligned}\quad (\text{E4})$$

Thereby, we have introduced

$$\begin{aligned}\hat{\mathcal{H}}_L(t) &= -h_x \hat{S}_x - (h_z + \mu\delta) \hat{S}_z + \epsilon \sum_a \hat{J}_{a,a}^+ \hat{J}_{a,a}^- \\ &+ \sum_a \frac{\Omega_{a,\chi}^*}{2} \hat{J}_{a,-a}^- e^{i\omega_p t} + \sum_a \frac{\Omega_{a,0}}{2} \hat{J}_{a,-a}^+ e^{-i\omega_p t},\end{aligned}\quad (\text{E5})$$

where the parameters are the same as in Eq. (D9). Moreover, $\hat{\mathcal{H}}_R(t) = \hat{\mathcal{H}}_L^\dagger(t) \Big|_{\chi \rightarrow -\chi, \delta \rightarrow -\delta}$.

To enable an efficient analysis of the system, we derive an effective Hamiltonian, which describes the collective dynamics in the ground-state manifold of the ensemble, in the same fashion as for the semiclassical model in Sec. D 2. To this end, we construct the Heisenberg equa-

tions of motion for the excitation operators,

$$\frac{d}{dt} \hat{J}_{-a,a}^- \approx -i(\epsilon_{\Delta} - i\frac{\Gamma}{2}) \hat{J}_{a,-a}^- - i\frac{\Omega_{a,0}}{2} \hat{P}_a, \quad (\text{E6})$$

where we have neglected incoherent terms in the same fashion as in Sec. D 2. Within an adiabatic approximation, we replace

$$J_{-a,a}^- \approx -\frac{1}{2} \frac{\Omega_{a,0}}{\epsilon_{\Delta} - i\frac{\Gamma}{2}} \hat{P}_a \quad (\text{E7})$$

in the master equation (E4). To project the dynamics on the ground-state manifold, we keep only the terms in Eq. (E4) whose final state is on the ground-state manifold. Thus, we keep terms like $\hat{J}^- \hat{J}^+ \rho$, while neglecting terms like $\hat{J}^+ \rho$ and $\hat{J}^+ \hat{J}^- \rho$. This procedure is on an equal footing with the ground-state-manifold projection in the semiclassical model in Sec. D 2. In doing so, we obtain the effective master equation

$$\begin{aligned}\mathcal{L}_{\chi}(t) \rho_{\chi} &= -i [\hat{\mathcal{H}}_L \rho_{\chi} - \rho_{\chi} \hat{\mathcal{H}}_R] \\ &+ \gamma_P D[\hat{S}_z + i\hat{S}_y] \rho_{\chi}, \\ &+ \frac{3\gamma_D}{\epsilon_{\Delta}^2 + \frac{\Gamma^2}{4}} \sum_a \Omega_{a,0}^* \Omega_{a,0} D[\hat{P}_a] \rho_{\chi} \\ &+ \frac{\Gamma}{\epsilon_{\Delta}^2 + \frac{\Gamma^2}{4}} \sum_a \Omega_{a,0} (\Omega_{a,\chi}^* - \Omega_{a,0}^*) \hat{P}_a \rho_{\chi} \\ &+ \frac{\Gamma}{\epsilon_{\Delta}^2 + \frac{\Gamma^2}{4}} \sum_a \Omega_{a,0}^* (\Omega_{a,\chi} - \Omega_{a,0}) \rho_{\chi} \hat{P}_a \\ &+ \frac{\gamma_z}{\epsilon_{\Delta}^2 + \frac{\Gamma^2}{4}} \sum_{\eta=\pm} \sum_{a=\pm 1} \Omega_{a,0}^* \Omega_{a,0} D_{\chi\eta} [\hat{P}_a] \rho_{\chi},\end{aligned}\quad (\text{E8})$$

where

$$\hat{\mathcal{H}}_L = -h_x \hat{S}_x - (h_z + \mu\delta) \hat{S}_z + (\mathcal{C}_{\chi} - \mathcal{C}_{-\chi}^*) \hat{S}_z \quad (\text{E9})$$

with \mathcal{C}_{χ} given in Eq. (D12). Note that we have assumed real valued Ω_x, Ω_y (corresponding to linearly polarized light) to bring the master equation in this form. Moreover, $\hat{\mathcal{H}}_R = \hat{\mathcal{H}}_L \Big|_{\chi \rightarrow -\chi, \delta \rightarrow -\delta}$. For $\chi_{\alpha} = \delta = 0$, we obtain the master equation in Eq. (23). We have phenomenologically added a pump term $\propto \gamma_P$ to establish a close connection to the semiclassical model in Eq. (D9). In the following, we set $\gamma_D = 0$ as it corresponds to spontaneous emission in an arbitrary direction. In contrast, we keep $\gamma_z > 0$ as it describes collective dissipation, necessary to microscopically describe quantum information in this system. Of note, the scaling factor $\Omega^2/\epsilon_{\Delta}^2 \approx 10^{-6}$ for the chosen parameters, such that the dissipator terms with \hat{P}_a become only important in the large atom number regime N .

2. Non-unitary mean-field theory

As the ensemble consists of a macroscopic number of atoms, we carry out a mean-field treatment to analyze the measurement statistics. As a first step, we apply the

Holstein-Primakoff transformation

$$\begin{aligned}\hat{S}_x &= \hat{a}^\dagger \hat{a} - \frac{N}{2}, \\ \hat{S}_+^{(x)} &= \hat{S}_z - i\hat{S}_y = \hat{a}^\dagger \sqrt{N - \hat{a}^\dagger \hat{a}}, \\ \hat{S}_-^{(x)} &= \hat{S}_z + i\hat{S}_y = \sqrt{N - \hat{a}^\dagger \hat{a}} \hat{a},\end{aligned}\quad (\text{E10})$$

where \hat{a} is a bosonic operator, and N denotes the total number of atoms in the ensemble. In terms of the Holstein-Primakoff boson, the generalized master equation reads

$$\begin{aligned}\frac{d}{dt}\rho_{\mathbf{x}} &= -i \left[-h_x \left(\hat{a}^\dagger \hat{a} - \frac{N}{2} \right) - (h_z + \mu\delta + \mathcal{C}_{\mathbf{x}} - \mathcal{C}_{-\mathbf{x}}^*) \frac{1}{2} \left(\hat{a}^\dagger \sqrt{N - \hat{a}^\dagger \hat{a}} + \sqrt{N - \hat{a}^\dagger \hat{a}} \hat{a} \right) \right] \rho_{\mathbf{x}} \\ &+ i\rho_{\mathbf{x}} \left[-h_x \left(\hat{a}^\dagger \hat{a} - \frac{N}{2} \right) - (h_z - \mu\delta - \mathcal{C}_{\mathbf{x}} + \mathcal{C}_{-\mathbf{x}}^*) \frac{1}{2} \left(\hat{a}^\dagger \sqrt{N - \hat{a}^\dagger \hat{a}} + \sqrt{N - \hat{a}^\dagger \hat{a}} \hat{a} \right) \right] \\ &+ \gamma_P \sqrt{N - \hat{a}^\dagger \hat{a}} \hat{a} \rho_{\mathbf{x}} \hat{a}^\dagger \sqrt{N - \hat{a}^\dagger \hat{a}} - \frac{\gamma_P}{2} (N - 1 - \hat{a}^\dagger \hat{a}) \hat{a}^\dagger \hat{a} \rho_{\mathbf{x}} - \frac{\gamma_P}{2} \rho_{\mathbf{x}} (N - 1 - \hat{a}^\dagger \hat{a}) \hat{a}^\dagger \hat{a} \\ &- \frac{\Gamma}{\epsilon_{\Delta}^2 + \frac{\Gamma^2}{4}} \sum_{a=\pm 1} \Omega_{a,0} \Omega_{a,\mathbf{x}}^* \left[\frac{N}{2} + \frac{a}{2} \left(\hat{a}^\dagger \sqrt{N - \hat{a}^\dagger \hat{a}} + \sqrt{N - \hat{a}^\dagger \hat{a}} \hat{a} \right) \right]^2 \rho_{\mathbf{x}} \\ &- \frac{\Gamma}{\epsilon_{\Delta}^2 + \frac{\Gamma^2}{4}} \sum_{a=\pm 1} \Omega_{a,0}^* \Omega_{a,\mathbf{x}} \rho_{\mathbf{x}} \left[\frac{N}{2} + \frac{a}{2} \left(\hat{a}^\dagger \sqrt{N - \hat{a}^\dagger \hat{a}} + \sqrt{N - \hat{a}^\dagger \hat{a}} \hat{a} \right) \right]^2 \\ &+ \frac{1}{\epsilon_{\Delta}^2 + \frac{\Gamma^2}{4}} \sum_{a=\pm 1} \Omega_{a,0}^* \Omega_{a,0} [3\gamma + \gamma_z (e^{-i\chi_x} + e^{-i\chi_y})] \\ &\times \left[\frac{N}{2} + \frac{a}{2} \left(\hat{a}^\dagger \sqrt{N - \hat{a}^\dagger \hat{a}} + \sqrt{N - \hat{a}^\dagger \hat{a}} \hat{a} \right) \right] \rho_{\mathbf{x}} \left[\frac{N}{2} + \frac{a}{2} \left(\hat{a}^\dagger \sqrt{N - \hat{a}^\dagger \hat{a}} + \sqrt{N - \hat{a}^\dagger \hat{a}} \hat{a} \right) \right].\end{aligned}\quad (\text{E11})$$

In contrast to the common mean-field theory in unitary systems, where one introduces a single mean field via a shift operation $\hat{a} \rightarrow \hat{a} + \alpha$ with a complex valued α , here we introduce four distinct complex mean fields $(\alpha_f, \alpha_{f*}, \alpha_b, \alpha_{b*}) = \alpha$, which we arrange as a vector for brevity [91]. These complex mean fields define the following non-unitary shift operations

$$\begin{aligned}\hat{W}_f &= \exp \left[\sqrt{N} (\alpha_{f*} \hat{a} - \alpha_f \hat{a}^\dagger) \right], \\ \hat{W}_b &= \exp \left[\sqrt{N} (\alpha_{b*} \hat{a} - \alpha_b \hat{a}^\dagger) \right].\end{aligned}\quad (\text{E12})$$

The labels f and b indicate that these operators are supposed to operate on the *front* or *back* side of the density matrix. Under these operations, the Holstein-Primakoff boson transforms as

$$\begin{aligned}\hat{W}_f \hat{a} \hat{W}_f^{-1} &= \hat{a} + \sqrt{N} \alpha_f, \\ \hat{W}_f \hat{a}^\dagger \hat{W}_f^{-1} &= \hat{a}^\dagger + \sqrt{N} \alpha_{f*}, \\ \hat{W}_b \hat{a} \hat{W}_b^{-1} &= \hat{a} + \sqrt{N} \alpha_b, \\ \hat{W}_b \hat{a}^\dagger \hat{W}_b^{-1} &= \hat{a}^\dagger + \sqrt{N} \alpha_{b*}.\end{aligned}\quad (\text{E13})$$

Using these shift operators, we define the non-unitary superoperator \mathcal{W} via the action on an density matrix

$$\mathcal{W}(\rho) = \hat{W}_f \rho \hat{W}_b^{-1}. \quad (\text{E14})$$

Accordingly, the inverse transformation is given by

$$\mathcal{W}^{-1}(\rho) = \hat{W}_f^{-1} \rho \hat{W}_b. \quad (\text{E15})$$

For instance, we have

$$\begin{aligned}\mathcal{W}(\hat{a} \rho \hat{a}^\dagger) &= \hat{W}_f \hat{a} \rho \hat{a} \hat{W}_b^{-1} \\ &= \hat{W}_f \hat{a} \hat{W}_f^{-1} \hat{W}_f \rho \hat{W}_b^{-1} \hat{W}_b \hat{a} \hat{W}_b^{-1} \\ &= (\hat{a} + \sqrt{N} \alpha_f) \tilde{\rho} (\hat{a}^\dagger + \sqrt{N} \alpha_{f*}) \\ &= N \alpha_f \alpha_{f*} \tilde{\rho} + \sqrt{N} (\alpha_{f*} \hat{a} \tilde{\rho} + \alpha_f \tilde{\rho} \hat{a}^\dagger) + \hat{a} \tilde{\rho} \hat{a}^\dagger,\end{aligned}\quad (\text{E16})$$

where $\tilde{\rho}$ is the density matrix in the transformed frame. In the last line, we have distributed the transformed operator in orders of the atom number. In the semiclassical limit $N \rightarrow \infty$, the first term will dominate, such that only the mean-field contribution is relevant.

Applying the transformation \mathcal{W} to the generalized master equation, we formally obtain

$$\begin{aligned} \frac{d}{dt}\rho_{\chi} &= \mathcal{L}_{\chi}\rho_{\chi} \\ &= \mathcal{W}^{-1}[\mathcal{W}(\mathcal{L}_{\chi}\rho_{\chi})] \\ &= N\lambda_{\chi}\mathcal{W}^{-1}[\tilde{\rho}_{\chi}] + \sqrt{N}\mathcal{W}^{-1}[\mathcal{L}_1\tilde{\rho}_{\chi}] + \mathcal{W}^{-1}[\mathcal{L}_2\tilde{\rho}_{\chi}] \\ &= N\lambda_{\chi}\rho_{\chi} + \sqrt{N}\mathcal{W}^{-1}[\check{\mathcal{L}}_1\tilde{\rho}_{\chi}] + \mathcal{W}^{-1}[\check{\mathcal{L}}_2\tilde{\rho}_{\chi}]. \end{aligned} \quad (\text{E17})$$

In the leading-order $\propto N$, the Liouvillian is thus just a complex-valued number λ_{χ} . To cancel the term $\propto \sqrt{N}$, we choose the mean field such that

$$\begin{aligned} 0 &= \mathcal{L}_1\tilde{\rho}_{\chi} \\ &= l_f(\boldsymbol{\alpha})\hat{a}\tilde{\rho}_{\chi} + l_{f*}(\boldsymbol{\alpha})\hat{a}^\dagger\tilde{\rho} + l_b(\boldsymbol{\alpha})\tilde{\rho}_{\chi}\hat{a} + l_{b*}(\boldsymbol{\alpha})\tilde{\rho}_{\chi}\hat{a}^\dagger, \end{aligned} \quad (\text{E18})$$

which gives four nonlinear equations [$l_f(\boldsymbol{\alpha}) = 0$ etc.] for four independent variables. These equations can be solved numerically.

In terms of the reduced density matrix, the time-evolution of the moment-generating function follows

$$\frac{d}{dt}M_{\text{dy},\chi} = \frac{d}{dt}\text{tr}[\rho_{\chi}]$$

$$\begin{aligned} \overline{K}_{\chi} &= -i \left[-h_x \left(\alpha_{f*}\alpha_f - \frac{1}{2} \right) - (h_z + \mu\delta + \mathcal{C}_{\chi} - \mathcal{C}_{-\chi}^*) \frac{1}{2} (\alpha_{f*}\sqrt{1 - \alpha_{f*}\alpha_f} + \sqrt{1 - \alpha_{f*}\alpha_f}\alpha_f) \right] \\ &+ i \left[-h_x \left(\alpha_{b*}\alpha_b - \frac{1}{2} \right) - (h_z - \mu\delta - \mathcal{C}_{\chi} + \mathcal{C}_{-\chi}^*) \frac{1}{2} (\alpha_{b*}\sqrt{1 - \alpha_{b*}\alpha_b} + \sqrt{1 - \alpha_{b*}\alpha_b}\alpha_b) \right] \\ &+ N\gamma_P\sqrt{1 - \alpha_{f*}\alpha_f}\alpha_f\alpha_{b*}\sqrt{1 - \alpha_{b*}\alpha_b} - N\frac{\gamma_P}{2} (1 - \alpha_{f*}\alpha_f)\alpha_{f*}\alpha_f - N\frac{\gamma_P}{2} (1 - \alpha_{b*}\alpha_b)\alpha_{b*}\alpha_b \\ &- \frac{N\Gamma}{\epsilon_{\Delta}^2 + \frac{\Gamma^2}{4}} \sum_{a=\pm 1} \Omega_{a,0}\Omega_{a,\chi}^* \left[\frac{1}{2} + \frac{a}{2} (\alpha_{f*}\sqrt{1 - \alpha_{f*}\alpha_f} + \sqrt{1 - \alpha_{f*}\alpha_f}\alpha_f) \right]^2 \\ &- \frac{N\Gamma}{\epsilon_{\Delta}^2 + \frac{\Gamma^2}{4}} \sum_{a=\pm 1} \Omega_{a,0}^*\Omega_{a,\chi} \left[\frac{1}{2} + \frac{a}{2} (\alpha_{b*}\sqrt{1 - \alpha_{b*}\alpha_b} + \sqrt{1 - \alpha_{b*}\alpha_b}\alpha_b) \right]^2 \\ &+ \frac{N}{\epsilon_{\Delta}^2 + \frac{\Gamma^2}{4}} \sum_{a=\pm 1} \Omega_{a,0}^*\Omega_{a,0} [3\gamma + \gamma_z (e^{-i\chi_x} + e^{-i\chi_y})] \\ &\quad \times \left[\frac{1}{2} + \frac{a}{2} (\alpha_{f*}\sqrt{1 - \alpha_{f*}\alpha_f} + \sqrt{1 - \alpha_{f*}\alpha_f}\alpha_f) \right] \left[\frac{1}{2} + \frac{a}{2} (\alpha_{b*}\sqrt{1 - \alpha_{b*}\alpha_b} + \sqrt{1 - \alpha_{b*}\alpha_b}\alpha_b) \right] \\ &+ \frac{1}{N} \sum_{\eta=x,y} (e^{-i\chi_{\eta}} - 1) \nu_{\eta}. \end{aligned} \quad (\text{E22})$$

Notably, this procedure can be amended with arbitrary operators (e.g., \hat{S}_y) by including the respective Holstein-Primakoff representation.

$$= N\lambda_{\chi}M_{\text{dy},\chi} + \text{tr}[\mathcal{W}^{-1}(\check{\mathcal{L}}_2\tilde{\rho}_{\chi})]. \quad (\text{E19})$$

Thus, the moment-generating function can be formally written as

$$M_{\text{dy},\chi}(t) = e^{N\lambda_{\chi}t}\check{M}_{\text{dy},\chi}(t), \quad (\text{E20})$$

where $\check{M}_{\text{dy},\chi}(t)$ contains contributions of order N^0 . This allows us to define an asymptotic cumulant-generating function in the thermodynamic limit $N \rightarrow \infty$ as

$$\begin{aligned} \overline{K}_{\chi} &\equiv \lim_{N \rightarrow \infty} \lim_{t \rightarrow \infty} \frac{1}{tN} \ln [M_{\text{dy},\chi}(t)M_{\chi}(0)] \\ &= \lambda_{\chi} + \frac{1}{N} \sum_{\eta} (e^{-i\chi_{\eta}} - 1) \dot{\bar{\nu}}_{\eta}, \end{aligned} \quad (\text{E21})$$

according to Eq. (B13) with $\dot{\bar{\nu}}_{\eta} = \bar{\nu}_{\eta}/t$ being the mean photon flux. For the generalized master equation in Eq. (E11), we formally assume that γ_P , γ_D and γ_z scale as N^{-1} to obtain a well-defined thermodynamic limit. Then, the asymptotic cumulant-generating function turns out to be

3. Efficient evaluation of low-order cumulants

In this Appendix, we explain how to efficiently calculate low-order cumulants of the measurement statistics. Crucially, the mean-fields appearing in Eq. (E11) are de-

terminated as the roots of l_f, l_{f*}, l_b, l_{b*} in Eq. (E18), and depend thus implicitly on the counting fields χ . This fact renders the evaluation of the derivatives of \bar{K}_χ with respect to the counting fields χ numerically unstable. For this reason, a more sophisticated evaluation method is required. For simplicity, we will focus on a single counting field in the following.

For brevity, we introduce $\alpha_1 = \alpha_f, \alpha_2 = \alpha_{f*}, \alpha_3 = \alpha_b, \alpha_4 = \alpha_{b*}$ and likewise for the l_f, l_{f*}, l_b, l_{b*} . We denote the roots of the l_i by $\alpha_i^{(0)}$ when $\chi = 0$, i.e.,

$$l_i(\boldsymbol{\alpha}^{(0)}) = 0, \quad (\text{E23})$$

and the same for the other mean fields. Moreover, for $\chi = 0$, we also find

$$\alpha_f^{(0)} = \alpha_{f*}^{(0)*} = \alpha_{b*}^{(0)*} = \alpha_b^{(0)},$$

which can be used to reduce the numerical effort.

Inspection of the expansion method further reveals that

$$\frac{\partial K_\chi}{\partial \alpha_i} = l_i(\boldsymbol{\alpha}) \quad (\text{E24})$$

for all i , which can be used to obtain the expansion coefficients in Eq. (E18) using a computer algebra system like *SymPy* or *Mathematica*.

The first total derivative of \bar{K}_χ with respect to the counting fields gives

$$\frac{d\bar{K}_\chi}{d\chi} = \frac{\partial \bar{K}_\chi}{\partial \alpha_i} \frac{\partial \alpha_i}{\partial \chi} + \frac{\partial \bar{K}_\chi}{\partial \chi}, \quad (\text{E25})$$

where $\partial/\partial\chi$ and $\partial/\partial\alpha_i$ denote partial derivatives. For brevity, we took advantage of the Einstein notation. Using Eqs. (E24) and (E23), we find that the first term on the right-hand side vanishes. Consequently, the first asymptotic cumulant is given by

$$\bar{\kappa}_1 = \frac{d\bar{K}_\chi}{d\chi} \Big|_{\chi=0} = \frac{\partial \bar{K}_\chi}{\partial \chi} \Big|_{\chi=0}, \quad (\text{E26})$$

where we recall that the cumulant-generating function has to be evaluated for $\alpha^{(0)}$.

The second total derivative yields

$$\frac{d^2\bar{K}_\chi}{d\chi^2} = \frac{\partial \bar{K}_\chi}{\partial \alpha_i \partial \alpha_j} \frac{\partial \alpha_i}{\partial \chi} \frac{\partial \alpha_j}{\partial \chi} + 2 \frac{\partial \bar{K}_\chi}{\partial \chi \partial \alpha_j} \frac{\partial \alpha_j}{\partial \chi} + \frac{\partial^2 \bar{K}_\chi}{\partial \chi^2}. \quad (\text{E27})$$

The evaluation requires the knowledge of $\frac{\partial \alpha_j}{\partial \chi} \Big|_{\chi=0}$, which we obtain as follows. Calculating the total derivatives of Eq. (E24) with respect to the counting field χ , we obtain

$$0 = \frac{d\bar{K}_\chi}{d\chi \partial \alpha_j} \Big|_{\chi=0}$$

$$= \frac{\partial \bar{K}_\chi}{\partial \alpha_j \partial \alpha_i} \frac{\partial \alpha_i}{\partial \chi} \Big|_{\chi=0} + \frac{\partial \bar{K}_\chi}{\partial \chi \partial \alpha_j} \Big|_{\chi=0}, \quad (\text{E28})$$

which is necessary zero when evaluated for a root α . This relation defines an inhomogeneous linear equation, which can be used to obtain the $\frac{\partial \alpha_j}{\partial \chi} \Big|_{\chi=0}$. Eventually, the asymptotic noise is thus given by

$$\begin{aligned} \bar{\kappa}_2 &= \frac{d^2 \bar{K}_\chi}{d\chi^2} \Big|_{\chi=0} \\ &= \frac{\partial \bar{K}_\chi}{\partial \chi \partial \alpha_j} \frac{\partial \alpha_j}{\partial \chi} \Big|_{\chi=0} + \frac{\partial^2 \bar{K}_\chi}{\partial \chi^2} \Big|_{\chi=0}. \end{aligned} \quad (\text{E29})$$

Of note, we can obtain the quantum Fisher information in exactly the same fashion when replacing the derivatives with respect to χ by derivatives with respect to δ . Likewise, we can also evaluate

$$\frac{d\kappa_1}{dh_z} = \frac{\partial \bar{K}_\chi}{\partial \chi \partial \alpha_j} \frac{\partial \alpha_j}{\partial h_z} \Big|_{\chi=0} + \frac{\partial^2 \bar{K}_\chi}{\partial \chi \partial h_z} \Big|_{\chi=0}, \quad (\text{E30})$$

where we obtain $\frac{\partial \alpha_j}{\partial h_z} \Big|_{\chi=0}$ by solving

$$0 = \frac{\partial \bar{K}_\chi}{\partial \alpha_j \partial \alpha_i} \frac{\partial \alpha_i}{\partial h_z} \Big|_{\chi=0} + \frac{\partial \bar{K}_\chi}{\partial h_z \partial \alpha_j} \Big|_{\chi=0}, \quad (\text{E31})$$

which is a linear inhomogeneous equation.

Interestingly, for a vanishing $B_z = 0$, we find that $\boldsymbol{\alpha} = 0$. For this reason, it is possible to evaluate the quantum Fisher information analytically, which give the result in Eq. (29).

4. Benchmark calculations

To validate the non-Hermitian mean-field theory, we compare the mean-field approach with exact numerical calculations of the finite-size model. To achieve a well-defined thermodynamic limit and for the simplicity of notation, we parameterize the generalized Liouvillian in Eq. (E8) as follows:

$$\begin{aligned} \frac{d}{dt} \rho &= -i \left[\hat{\mathcal{H}}_L \rho - \rho \hat{\mathcal{H}}_R \right] \\ &+ \frac{\kappa_P}{N} D[\hat{S}_z + i\hat{S}_y] \rho, \\ &+ \frac{\kappa_z}{N} \sum_a D \left[\hat{P}_a \right] \rho, \end{aligned} \quad (\text{E32})$$

For the benchmarking, we will consider the quantum Fisher information, such that we set $\chi = 0$. Please note that the Hamiltonians $\hat{\mathcal{H}}_L, \hat{\mathcal{H}}_R$ given in Eq. (E9) still depend on the auxiliary variable δ , required for the evaluation the quantum Fisher information. We recall that the quantum Fisher information can be numerically obtained for finite-size systems by evaluating Eq. (A11).

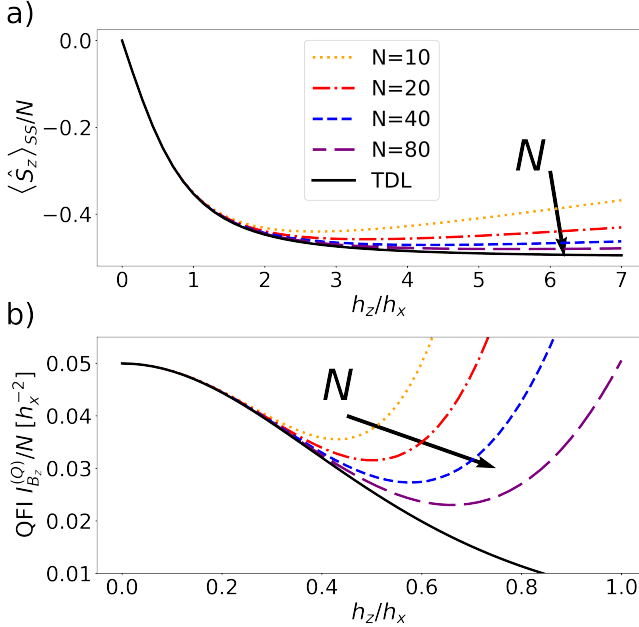


FIG. 4. Benchmark calculations of the collective model in Eq. (E32). (a) Expectation value of \hat{S}_z as a function of h_z for four different atom numbers $N = 10, 20, 40, 80$ and fixed $\kappa_z = 0$ and $\kappa_D = 0.01h_x$. The solid black line depicts the mean-field result using the asymptotic cumulant-generating function in Eq. (E22). (b) shows the same as (a), but for the quantum Fisher information.

For simplicity, we have introduced the effective parameters

$$\begin{aligned} \kappa_P &= N\gamma_P, \\ \kappa_z &= N\gamma_z \frac{\Omega^2}{\epsilon_\Delta^2 + \frac{\gamma_z^2}{4}}, \end{aligned} \quad (E33)$$

for which the system in Eq. (E32) reaches a well-defined thermodynamic limit.

In Fig. 4(a), we depict the expectation value of \hat{S}_z as a function of h_z for atom numbers $N = 10, 20, 40, 80$. We observe that the mean-field approach representing the thermodynamic limit $N \rightarrow \infty$ agrees closely to the finite-size calculations for small h_z , while there are significant deviations for larger h_z . Yet, the finite-size calculation gradually approaches the mean-field result with increasing atom number. In Fig. 4(b), we investigate the quantum Fisher information as a function of h_z . As in panel (a), the finite-size results converge significantly faster to the mean-field result for smaller h_z . Note the different plot ranges in panels (a) and (b), which suggests that fluctuations (such as the Fisher information) require a higher atom number for convergence than expectation

values. Crucially, the mean-field treatment works excellently for $h_z = 0$, which is the main focus of this investigation.

In Fig. 5, we analyze the convergence of the finite-size calculations as a function of the effective dissipation κ_z for $h_z = 0$. In Fig. 5(a), we investigate the expectation value of \hat{S}_x . Crucially, the numerical solution of Eq. (E23) is given by $\alpha^{(0)} = \mathbf{0}$, which corresponds to $\langle \hat{S}_x \rangle / N = -0.5$. For small κ_z , the finite-size calculations has already converged to this value, while for large κ_z we observe $\langle \hat{S}_x \rangle = 0$. For intermediate κ_z , we find that the crossover point between the $\langle \hat{S}_x \rangle = 0$ and $\langle \hat{S}_x \rangle / N = -0.5$ regimes linearly increases towards larger κ_z for increasing atom number N .

In Fig. 5(c), we depict the quantum Fisher information as a function of κ_z for $h_z = 0$. Assuming that $\alpha^{(0)} = \mathbf{0}$, we can find an analytical expression of the quantum Fisher information in the thermodynamic limit using the methods in App. E 3, which is given in Eq. (29) and depicted in Fig. 5(c). For small κ_z we find that the quantum Fisher information in the thermodynamic limit is independent of κ_z and agrees perfectly with the finite-size calculations.

For intermediate $\kappa_z \approx 0.1h_x$, we observe finite deviations in the crossover regime from $\langle \hat{S}_x \rangle / N = -0.5$ to $\langle \hat{S}_x \rangle = 0$. As the mean-field approach assumes $\langle \hat{S}_x \rangle / N = -0.5$, the mean-field approach in App. (E2) is invalid, explaining the deviations between the analytical and numerical calculations. Crucially, deviations gradually vanish with increasing atom number.

For larger $\kappa_z \approx 0.1h_x$ we find a linear dependence of both the thermodynamic-limit and finite-size calculations, which differ by a constant factor. For very large $\kappa_z \gg 0.1h_x$, the finite-size calculations quickly approach a linear asymptotic behavior. According to Fig. 5(a) and using that $\langle \hat{S}_y \rangle = \langle \hat{S}_z \rangle = 0$ (not shown), we find that the mean value is located at the center of the Bloch sphere in this exotic asymptotic regime. As the mean-field approach in App. E 2 can only represent mean macroscopic spin states on the surface of the Bloch sphere, it fails to agree with finite-size calculations in this atom-number regime.

Interestingly, the comparison of the thermodynamic-limit and finite-size calculations in the linear scaling regime for large κ_z reveals that both values are identical up to a constant factor $\sqrt{8}$, which we confirmed by comparing various system parameters. Thus, the large κ_z range constitutes a *pre-convergence* regime, in which we find exactly the same scaling properties as in the fully converged system.

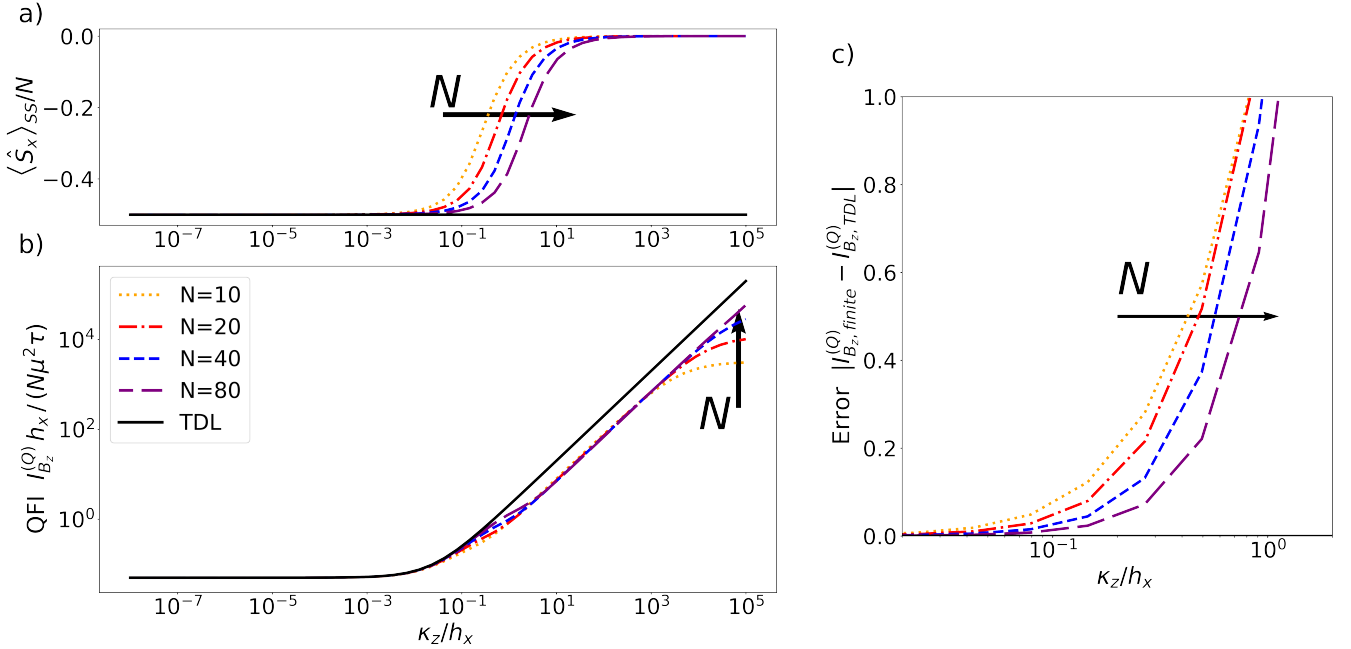


FIG. 5. Expectation value of \hat{S}_x as a function of κ_z for $h_z = 0$, $\kappa_P = 0.1h_x$ and atom numbers $N = 10, 20, 40, 80$. The solid black line depicts the mean-field result representing the thermodynamic limit (TDL). (b) Quantum Fisher information for the finite-size system (colored lines) and in the thermodynamic limit given by Eq. (29) (black). (c) Deviation between the finite-size and thermodynamic-limit calculations in (b) in the crossover regime.

[1] J. Ye and P. Zoller, Essay: Quantum sensing with atomic, molecular, and optical platforms for fundamental physics, *Phys. Rev. Lett.* **132**, 190001 (2024).

[2] C. L. Degen, F. Reinhard, and P. Cappellaro, Quantum sensing, *Rev. Mod. Phys.* **89**, 035002 (2017).

[3] A. D. Ludlow, M. M. Boyd, J. Ye, E. Peik, and P. O. Schmidt, Optical atomic clocks, *Rev. Mod. Phys.* **87**, 637 (2015).

[4] G. Hoth, A. Radnaev, P. Mitchell, J. Sherman, and V. Gerginov, "NIST-F3, a cesium fountain frequency reference", in *Proceedings of the 54th Annual Precise Time and Time Interval Systems and Applications (PTTI) Meeting* (2024) pp. 183–188.

[5] S. M. Brewer, J.-S. Chen, A. M. Hankin, E. R. Clements, C. W. Chou, D. J. Wineland, D. B. Hume, and D. R. Leibrandt, $^{27}\text{Al}^+$ Quantum-Logic Clock with a Systematic Uncertainty below 10^{-18} , *Phys. Rev. Lett.* **123**, 033201 (2019).

[6] N. Ji, Y. Liang, W. Yu, Q. Yin, and T. Vogt, Optimizing four-wave mixing in Rydberg atoms for microwave-optical conversion, *Phys. Rev. A* **110**, 052608 (2024).

[7] D. H. Meyer, Z. A. Castillo, K. C. Cox, and P. D. Kunz, Assessment of Rydberg atoms for wideband electric field sensing, *Journal of Physics B: Atomic, Molecular and Optical Physics* **53**, 034001 (2020).

[8] M. Jing, Y. Hu, J. Ma, H. Zhang, L. Zhang, L. Xiao, and S. Jia, Atomic superheterodyne receiver based on microwave-dressed Rydberg spectroscopy, *Nature Physics* **16**, 911 (2020).

[9] D. Li, Z. Bai, X. Zuo, Y. Wu, J. Sheng, and H. Wu, Room temperature single-photon terahertz detection with thermal rydberg atoms, *Applied Physics Reviews* **11**, 041420 (2024).

[10] G. Engelhardt, K. Dorfman, and Z. Zhang, Photon-resolved floquet theory approach to spectroscopic quantum sensing, *Phys. Rev. A* **112**, 063725 (2025).

[11] K. E. Dorfman, S. Asban, B. Gu, and S. Mukamel, Hong-Ou-Mandel interferometry and spectroscopy using entangled photons, *Communications Physics* **4**, 49 (2021).

[12] Z. Zhang, T. Peng, X. Nie, G. S. Agarwal, and M. O. Scully, Entangled photons enabled time-frequency-resolved coherent Raman spectroscopy and applications to electronic coherences at femtosecond scale, *Light: Science and Applications* **11**, 10.1038/s41377-022-00953-y (2022).

[13] T. Li, F. Li, X. Liu, V. V. Yakovlev, and G. S. Agarwal, Quantum-enhanced stimulated Brillouin scattering spectroscopy and imaging, *Optica* **9**, 959 (2022).

[14] Z. Zhang, X. Zhang, J. Liu, and H. Dong, Quantum-enhanced weak absorption estimation with correlated photons, *Phys. Rev. Lett.* **134**, 133604 (2025).

[15] A. L. Bloom, Principles of operation of the rubidium vapor-magnetometer, *Appl. Opt.* **1**, 61 (1962).

[16] J. C. Allred, R. N. Lyman, T. W. Kornack, and M. V. Romalis, High-sensitivity atomic magnetometer unaffected by spin-exchange relaxation, *Phys. Rev. Lett.* **89**, 130801 (2002).

[17] V. Shah, S. Knappe, P. D. D. Schwindt, and J. Kitch-

ing, Subpicotesla atomic magnetometry with a microfabricated vapour cell, *Nature Photonics* **1**, 649 (2007).

[18] F. Wolfgramm, A. Cerè, F. A. Beduini, A. Predojević, M. Koschorreck, and M. W. Mitchell, Squeezed-light optical magnetometry, *Phys. Rev. Lett.* **105**, 053601 (2010).

[19] D. Budker and D. F. Jackson Kimball, eds., *Optical Magnetometry* (Cambridge University Press, 2013).

[20] R. Jiménez-Martínez, J. Kołodyński, C. Troullinou, V. G. Lucivero, J. Kong, and M. W. Mitchell, Signal tracking beyond the time resolution of an atomic sensor by kalman filtering, *Phys. Rev. Lett.* **120**, 040503 (2018).

[21] Y. Cohen, K. Jadeja, S. Sula, M. Venturelli, C. Deans, L. Marmugi, and F. Renzoni, A cold atom radio-frequency magnetometer, *Applied Physics Letters* **114**, 073505 (2019).

[22] Y. Ma, Y. Chen, M. Yu, Y. Wang, S. Lu, J. Guo, G. Luo, L. Zhao, P. Yang, Q. Lin, and Z. Jiang, Ultrasensitive serif atomic magnetometer with a miniaturized hybrid vapor cell, *Microsystems and Nanoengineering* **10**, 121 (2024).

[23] H. Bao, J. Duan, S. Jin, X. Lu, P. Li, W. Qu, M. Wang, I. Novikova, E. E. Mikhailov, K.-F. Zhao, K. Mølmer, H. Shen, and Y. Xiao, Spin squeezing of 10^{11} atoms by prediction and retrodiction measurements, *Nature* **581**, 159 (2020).

[24] S. Jin, J. Duan, Y. Zhang, X. Zhang, H. Bao, H. Shen, L. Xiao, S. Jia, M. Wang, and Y. Xiao, Concurrent spin squeezing and light squeezing in an atomic ensemble, *Phys. Rev. Lett.* **133**, 173604 (2024).

[25] B. Babaei, B. D. Smith, A. Tretiakov, A. Narayanan, and L. J. LeBlanc, Microwave-optical double-resonance vector magnetometry with warm rb atoms (2025), arXiv:2507.08791 [physics.atom-ph].

[26] K. Hammerer, A. S. Sørensen, and E. S. Polzik, Quantum interface between light and atomic ensembles, *Rev. Mod. Phys.* **82**, 1041 (2010).

[27] B. Chen, C. Qiu, S. Chen, J. Guo, L. Q. Chen, Z. Y. Ou, and W. Zhang, Atom-light hybrid interferometer, *Phys. Rev. Lett.* **115**, 043602 (2015).

[28] X. Wang, J. Wang, Z. Ren, R. Wen, C.-L. Zou, G. A. Siviloglou, and J. F. Chen, Quantum interference between photons and single quanta of stored atomic coherence, *Phys. Rev. Lett.* **128**, 083605 (2022).

[29] I. M. Bloch, Y. Hochberg, E. Kuflik, and T. Volansky, Axion-like relics: new constraints from old comagnetometer data, *Journal of High Energy Physics* **2020**, 167 (2020).

[30] S. Afach, B. C. Buchler, D. Budker, C. Dailey, A. Derevianko, V. Dumont, N. L. Figueroa, I. Gerhardt, Z. D. Grujić, H. Guo, C. Hao, P. S. Hamilton, M. Hedges, D. F. Jackson Kimball, D. Kim, S. Khamis, T. Kornack, V. Lebedev, Z.-T. Lu, H. Masia-Roig, M. Monroy, M. Padniuk, C. A. Palm, S. Y. Park, K. V. Paul, A. Penaflo, X. Peng, M. Pospelov, R. Preston, S. Pustelny, T. Scholtes, P. C. Segura, Y. K. Semertzidis, D. Sheng, Y. C. Shin, J. A. Smiga, J. E. Stalnaker, I. Sulai, D. Tandon, T. Wang, A. Weis, A. Wickenbrock, T. Wilson, T. Wu, D. Wurm, W. Xiao, Y. Yang, D. Yu, and J. Zhang, Search for topological defect dark matter with a global network of optical magnetometers, *Nature Physics* **17**, 1396 (2021).

[31] I. M. Bloch, G. Ronen, R. Shaham, O. Katz, T. Volansky, and O. Katz, New constraints on axion-like dark matter using a Floquet quantum detector, *Science Advances* **8**, eab18919 (2022).

[32] C. B. Møller, R. A. Thomas, G. Vasilakis, E. Zeuthen, Y. Tsaturyan, M. Balabas, K. Jensen, A. Schliesser, K. Hammerer, and E. S. Polzik, Quantum back-action-evading measurement of motion in a negative mass reference frame, *Nature* **547**, 191 (2017).

[33] F. Y. Khalili and E. S. Polzik, Overcoming the standard quantum limit in gravitational wave detectors using spin systems with a negative effective mass, *Phys. Rev. Lett.* **121**, 031101 (2018).

[34] J. Jia, V. Novikov, T. B. Brasil, E. Zeuthen, J. H. Müller, and E. S. Polzik, Acoustic frequency atomic spin oscillator in the quantum regime, *Nature Communications* **14**, 6396 (2023).

[35] V. Novikov, J. Jia, T. B. Brasil, A. Grimaldi, M. Bocoum, M. Balabas, J. H. Müller, E. Zeuthen, and E. S. Polzik, Hybrid quantum network for sensing in the acoustic frequency range, *Nature* **643**, 955 (2025).

[36] H. Cramér, *Mathematical Methods of Statistics* (Princeton University Press, Princeton, 1946).

[37] C. R. Rao, Information and accuracy attainable in the estimation of statistical parameters, *Bull. Calcutta Math. Soc.* **37**, 81 (1945).

[38] C. Helstrom, Minimum mean-squared error of estimates in quantum statistics, *Physics Letters A* **25**, 101 (1967).

[39] M. Hayashi, *Quantum Information Theory* (Springer Berlin, Heidelberg, 2017).

[40] V. Giovannetti, S. Lloyd, and L. Maccone, Quantum-enhanced measurements: Beating the standard quantum limit, *Science* **306**, 1330 (2004).

[41] R. Liu, Y. Chen, M. Jiang, X. Yang, Z. Wu, Y. Li, H. Yuan, X. Peng, and J. Du, Experimental critical quantum metrology with the Heisenberg scaling, *npj Quantum Information* **7**, 170 (2021).

[42] R. Di Candia, F. Minganti, K. V. Petrovnik, G. S. Paraoanu, and S. Felicetti, Critical parametric quantum sensing, *npj Quantum Information* **9**, 23 (2023).

[43] L. Qin, J. Li, Y. Niu, and X.-Q. Li, Enhanced super-Heisenberg scaling precision by nonlinear coupling and postselection, *Physics Letters A* **523**, 129795 (2024).

[44] M. Block, B. Ye, B. Roberts, S. Chern, W. Wu, Z. Wang, L. Pollet, E. J. Davis, B. I. Halperin, and N. Y. Yao, Scalable spin squeezing from finite-temperature easy-plane magnetism, *Nature Physics* **20**, 1575 (2024).

[45] S. Sarkar, A. Bayat, S. Bose, and R. Ghosh, Exponentially-enhanced quantum sensing with many-body phase transitions, *Nature Communications* **16**, 5159 (2025).

[46] M. Malnou, D. A. Palken, B. M. Brubaker, L. R. Vale, G. C. Hilton, and K. W. Lehnert, Squeezed vacuum used to accelerate the search for a weak classical signal, *PRX* **9**, 021023 (2019).

[47] M. Gessner, A. Smerzi, and L. Pezzè, Multiparameter squeezing for optimal quantum enhancements in sensor networks, *Nature Communications* **11**, 3817 (2020).

[48] K. M. Backes, D. A. Palken, S. A. Kenany, B. M. Brubaker, S. B. Cahn, A. Droster, G. C. Hilton, S. Ghosh, H. Jackson, S. K. Lamoreaux, A. F. Leder, K. W. Lehnert, S. M. Lewis, M. Malnou, R. H. Maruyama, N. M. Rapidis, M. Simanovskaia, S. Singh, D. H. Speller, I. Urdinaran, L. R. Vale, E. C. van Assendelft, K. van Bibber, and H. Wang, A quantum enhanced search for dark matter axions, *Nature* **590**, 238 (2021).

[49] T.-W. Mao, Q. Liu, X.-W. Li, J.-H. Cao, F. Chen, W.-

X. Xu, M. K. Tey, Y.-X. Huang, and L. You, Quantum-enhanced sensing by echoing spin-nematic squeezing in atomic Bose-Einstein condensate, *Nature Physics* **19**, 1585 (2023).

[50] E. M. Kessler, P. Kómár, M. Bishof, L. Jiang, A. S. Sørensen, J. Ye, and M. D. Lukin, Heisenberg-limited atom clocks based on entangled qubits, *Phys. Rev. Lett.* **112**, 190403 (2014).

[51] P. Kómár, E. M. Kessler, M. Bishof, L. Jiang, A. S. Sørensen, J. Ye, and M. D. Lukin, A quantum network of clocks, *Nature Physics* **10**, 582 (2014).

[52] R. Demkowicz-Dobrzański and L. Maccone, Using entanglement against noise in quantum metrology, *Phys. Rev. Lett.* **113**, 250801 (2014).

[53] R. Demkowicz-Dobrzański, J. Czajkowski, and P. Sekatski, Adaptive quantum metrology under general Markovian noise, *Phys. Rev. X* **7**, 041009 (2017).

[54] S. Zhou, M. Zhang, J. Preskill, and L. Jiang, Achieving the Heisenberg limit in quantum metrology using quantum error correction, *Nature Communications* **9**, 78 (2018).

[55] N. Didier, F. Qassemi, and A. Blais, Perfect squeezing by damping modulation in circuit quantum electrodynamics, *Phys. Rev. A* **89**, 013820 (2014).

[56] A. Blais, A. L. Grimsmo, S. M. Girvin, and A. Wallraff, Circuit quantum electrodynamics, *Rev. Mod. Phys.* **93**, 025005 (2021).

[57] T. Ilias, D. Yang, S. F. Huelga, and M. B. Plenio, Criticality-enhanced quantum sensing via continuous measurement, *PRX Quantum* **3**, 010354 (2022).

[58] A. Cabot, F. Carollo, and I. Lesanovsky, Continuous sensing and parameter estimation with the boundary time crystal, *Phys. Rev. Lett.* **132**, 050801 (2024).

[59] W. Qin, A. Miranowicz, and F. Nori, Exponentially improved dispersive qubit readout with squeezed light, *Phys. Rev. Lett.* **133**, 233605 (2024).

[60] L. K. Thomsen, S. Mancini, and H. M. Wiseman, Spin squeezing via quantum feedback, *Phys. Rev. A* **65**, 061801 (2002).

[61] J. Geremia, J. K. Stockton, A. C. Doherty, and H. Mabuchi, Quantum kalman filtering and the heisenberg limit in atomic magnetometry, *Phys. Rev. Lett.* **91**, 250801 (2003).

[62] K. Mølmer and L. B. Madsen, Estimation of a classical parameter with Gaussian probes: Magnetometry with collective atomic spins, *Phys. Rev. A* **70**, 052102 (2004).

[63] L. B. Madsen and K. Mølmer, Spin squeezing and precision probing with light and samples of atoms in the gaussian description, *Phys. Rev. A* **70**, 052324 (2004).

[64] C. Zhang and K. Mølmer, Estimating a fluctuating magnetic field with a continuously monitored atomic ensemble, *Phys. Rev. A* **102**, 063716 (2020).

[65] H. M. Wiseman and G. J. Milburn, Quantum theory of field-quadrature measurements, *Phys. Rev. A* **47**, 642 (1993).

[66] H. Wiseman and G. Milburn, *Quantum measurement and control* (Cambridge University Press, New York, 2010).

[67] G. T. Landi, M. J. Kewming, M. T. Mitchison, and P. P. Potts, Current fluctuations in open quantum systems: Bridging the gap between quantum continuous measurements and full counting statistics, *PRX Quantum* **5**, 020201 (2024).

[68] C. Schön, E. Solano, F. Verstraete, J. I. Cirac, and M. M. Wolf, Sequential generation of entangled multi-qubit states, *Phys. Rev. Lett.* **95**, 110503 (2005).

[69] J. I. Cirac, D. Pérez-García, N. Schuch, and F. Verstraete, Matrix product states and projected entangled pair states: Concepts, symmetries, theorems, *Rev. Mod. Phys.* **93**, 045003 (2021).

[70] D. Yang, S. F. Huelga, and M. B. Plenio, Efficient information retrieval for sensing via continuous measurement, *Phys. Rev. X* **13**, 031012 (2023).

[71] S. Mukamel, *Principles of nonlinear optical spectroscopy* (OXFORD UNIVERSITY PRESS, 1995).

[72] M. O. Scully and M. S. Zubairy, *Quantum optics* (Cambridge University Press, 1997).

[73] S. Pustelnik, W. Gawlik, S. M. Rochester, D. F. J. Kimball, V. V. Yashchuk, and D. Budker, Nonlinear magneto-optical rotation with modulated light in tilted magnetic fields, *Phys. Rev. A* **74**, 063420 (2006).

[74] M. Auzinsh, D. Budker, and S. Rochester, *Optically Polarized Atoms: Understanding light-atom interactions* (Oxford University Press, 2010).

[75] A. e. a. Akbar, Optimized detection modality for radio-frequency sensing with a double-resonance alignment magnetometer, *Phys. Rev. Appl.* **22**, 054033 (2024).

[76] J. M. Robinson, M. Miklos, Y. M. Tso, C. J. Kennedy, T. Bothwell, D. Kedar, J. K. Thompson, and J. Ye, Direct comparison of two spin-squeezed optical clock ensembles at the 10^{-17} level, *Nature Physics* **20**, 208 (2024).

[77] G. Ferioli, A. Glicenstein, I. Ferrier-Barbut, and A. Browaeys, A non-equilibrium superradiant phase transition in free space, *Nature Physics* **19**, 1345 (2023).

[78] S. Agarwal, E. Chaparro, D. Barberena, A. P. n. Orioli, G. Ferioli, S. Pancaldi, I. Ferrier-Barbut, A. Browaeys, and A. Rey, Directional superradiance in a driven ultracold atomic gas in free space, *PRX Quantum* **5**, 040335 (2024).

[79] D. Goncalves, L. Bombieri, G. Ferioli, S. Pancaldi, I. Ferrier-Barbut, A. Browaeys, E. Shahmoon, and D. Chang, Driven-dissipative phase separation in free-space atomic ensembles, *PRX Quantum* **6**, 020303 (2025).

[80] W. Górecki, F. Albarelli, S. Felicetti, R. Di Candia, and L. Maccone, Interplay between time and energy in bosonic noisy quantum metrology, *PRX Quantum* **6**, 020351 (2025).

[81] S. Gammelmark and K. Mølmer, Fisher information and the quantum Cramér-Rao sensitivity limit of continuous measurements, *Phys. Rev. Lett.* **112**, 170401 (2014).

[82] X. J. Liu, M. Ding, Y. Li, W. Hu, Y. H. and Jin, and J. C. Fang, Transverse relaxation determination based on light polarization modulation for spin-exchange relaxation free atomic magnetometer, *Chinese Physics B* **27**, 073201 (2018).

[83] S. P. Alvarez, P. Gomez, S. Coop, R. Zamora-Zamora, C. Mazzinghi, and M. W. Mitchell, Single-domain bose condensate magnetometer achieves energy resolution per bandwidth below $\Delta E / E \approx 10^{-10}$, *Proceedings of the National Academy of Sciences* **119**, e2115339119 (2022), <https://www.pnas.org/doi/pdf/10.1073/pnas.2115339119>.

[84] G. Engelhardt, J. Luo, V. M. Bastidas, and G. Platero, Photon-resolved Floquet theory. II. Open quantum systems, *Phys. Rev. A* **110**, 063708 (2024).

[85] M. Radaelli, G. T. Landi, K. Modi, and F. C. Binder, Fisher information of correlated stochastic processes, *New Journal of Physics* **25**, 053037 (2023).

[86] J. Kong, R. Jiménez-Martínez, C. Troullinou, V. G.

Lucivero, G. Tóth, and M. W. Mitchell, Measurement-induced, spatially-extended entanglement in a hot, strongly-interacting atomic system, *Nature Communications* **11**, 2415 (2020).

[87] B. Windt, M. Bello, D. Malz, and J. I. Cirac, Effects of retardation on many-body superradiance in chiral waveguide qed, *Phys. Rev. Lett.* **134**, 173601 (2025).

[88] Numerical data and source code can be downloaded from www.georg-engelhardt-research.de.

[89] A. A. Clerk, M. H. Devoret, S. M. Girvin, F. Marquardt, and R. J. Schoelkopf, Introduction to quantum noise, measurement, and amplification, *Rev. Mod. Phys.* **82**, 1155 (2010).

[90] D. A. Bagrets and Y. V. Nazarov, Full counting statistics of charge transfer in Coulomb blockade systems, *Phys. Rev. B* **67**, 085316 (2003).

[91] M. Li, L. JY., G. Platero, and G. Engelhardt, Full-counting statistics and quantum information of dispersive readout with a squeezed environment, to be published (2025).